Applied Chemistry

Olefin Purification and Selective Hydrogenation of Alkynes with Low Loaded Pd Nanoparticle Catalysts

Misael Cordoba, Fernando Coloma-Pascual, Mónica Esther Quiroga, and Cecilia Rosa Rosa Lederhos

Ind. Eng. Chem. Res., **Just Accepted Manuscript** • DOI: 10.1021/acs.iecr.9b02081 • Publication Date (Web): 16 Aug 2019

Olefin Purification and Selective Hydrogenation of Alkynes with Low Loaded Pd Nanoparticle Catalysts

*Misael Cordoba[1], Fernando Coloma-Pascual[2], Mónica E. Quiroga[1,3], Cecilia R. Lederhos[1,]**

[1] Instituto de Investigaciones en Catálisis y Petroquímica, INCAPE (FIQ-UNL, CONICET), Colectora Ruta Nac. N° 168 Km 0, Pje El Pozo, 3000 Santa Fe, Argentina.

[2] Servicios Técnicos de Investigación, Facultad de Ciencias, Universidad de Alicante, Apartado 99, E-03080 Alicante, Spain.

[3] Facultad de Ingeniería Química, Universidad Nacional del Litoral, Santiago del Estero 2829, 3000 Santa Fe, Argentina.

** E-mail: clederhos@fiq.unl.edu.ar*

KEYWORDS: Selective Hydrogenation, Alkynes, Olefin Purification, Lindlar, Palladium Nanoparticles.

ABSTRACT

The catalytic performance of Pd-nanoparticle catalysts for the selective hydrogenation of alkynes at mild conditions (150 kPa and 303 K) was evaluated. A Lindlar commercial catalyst was also

tested for comparison. The effects of acidity, amount of active sites and dispersion on the catalytic activity and selectivity were studied. At mild conditions, Pd-nanoparticle catalysts were considerably more active and slightly more selective than the Lindlar catalyst. The best synthesized catalyst for the purification of 1-pentene was Pd/Al_2O_3–Mg (r^0= 41.1 mol $g_{Pd}^{-1}min^{-1}$, 94% selectivity). The activity and selectivity of $Pd/CaCO_3$ were similar to those of the Lindlar catalyst. The smallest particle sizes (3-4.5 nm) favored the dissociative adsorption of hydrogen over Pd° active sites and a good catalytic behavior. The weaker acid centers (Lewis) of Pd/Al_2O_3–Mg and $Pd/CaCO_3$ favored higher selectivities to the desired alkene. Pd/Al_2O_3 was the most active catalyst but also the least selective. This was due to strong acid sites, remnant Bronsted acid sites, which provide extra hydrogen that favors the alkyne hydrogenation rate and also the undesired overhydrogenation of the alkene and/or the isomerization.

1. Introduction

Olefins are very important products for the industries of fine chemicals, petrochemicals and polymers[1, 2]. Industrial synthesis of alkenes can be carried out by several synthesis routes. In general lower molecular weight alkenes can be obtained in the petrochemical industry while higher alkenes can be synthesized through derivatives of this industry and by other methods[3]. Some of these processes include thermal treatment, dehydrogenation, catalytic cracking and hydrogenation[2, 4, 5]. After these processes not only desirable products are obtained, undesired products may also be present as alkanes, alkynes or other unsaturated products[6, 7]. Selective hydrogenation is a key process for the elimination of impurities or the obtaining of products with high added value. All selective hydrogenations are of great interest considering economic and ecological aspects[2, 8, 9]. Selective hydrogenation of alkynes to alkenes represents one of the most important steps in fine chemicals manufacture[10]. The highly selective hydrogenation of C≡C

triple bonds (alkynes) in presence of C=C double bonds (alkenes) is of great relevance in order to obtain streams enriched in olefins for different processes[11-14]. The selective hydrogenation of small alkynes and alkadienes (acetylene, propyne, butyne) for the purification of olefin streams has been studied extensively[15-17]. Hydrogenation of bigger compounds is of great importance but has been studied less[18-21].

Several authors have studied reactions of selective hydrogenation of medium to high molecular weight alkynes (C_5 - C_7[18, 19, 22-24], 3-methyl-1-pentyn-3-ol[25], 2-methyl-3-butyn-2-ol[20, 26], phenyl acetylene[27] and others[28]). Jackson et al.[24, 29-31] studied the hydrogenation of alkynes/alkenes mixtures. They focused systematically on the selective hydrogenation of higher molecular weight alkynes, obtaining several important results about the reaction kinetics[29-32]. Murugesan et al.[33] studied the elimination of phenylacetylene in the presence of styrene. Using Ni-fructose @ SiO_2-800, 0.5 mmol of phenylacetylene (5%) were hydrogenated in the presence of 9.5 mmol of styrene (95%) at 353 K with 1 MPa H_2 pressure. At these reaction conditions phenylacetylene was converted to 97% styrene and 3% ethylbenzene.

Palladium is widely used in hydrogenation reactions due to its high hydrogenating capacity, being active and selective at low temperatures[19, 34, 35]. Overhydrogenation should however be avoided. Different factors can be manipulated to control Pd catalytic activity and selectivity: metal precursor salt, support, impregnation method, particle size and dispersion, and reaction conditions[36, 37]. The classical Lindlar catalyst, consisting of $Pd_{(5\%)}$ supported on $CaCO_3$ poisoned with a lead promoter (which greatly increases its selectivity), has been used since 1954[38, 39]. Some disadvantages of this catalyst are: i) it has a high cost due to its high metal load, ii) it cannot be pelletized thus preventing easy separation and reuse, iii) restricted use, especially for the manufacture of food, cosmetic and medicine, because of the leaching of extremely toxic lead

compounds. There is therefore a challenge for synthesizing new catalysts without these drawbacks and that can also improve the performance of Lindlar catalysts with comparable or higher selectivity to the desired product during hydrogenation processes of medium/large molecular weight alkynes. Several supported Pd catalysts have been prepared and evaluated for the selective hydrogenation of olefins, e.g. $Pd_{(1\%)}$/Hydrotalcite[40], Pd_4S/carbon nanofiber[6] and different bimetallic catalysts, $Pd_{(0.4\%)}$-$Ni_{(0.5\text{-}1\%)}$[35, 41], $Pd_{(0.5\%)}$-$In_{(0.4\%)}$[42], $Pd_{(1\text{-}5\%)}$-Bi[43]. The kind of support can improve or decrease the activity/selectivity of the catalysts. Thus several supports have been tried to improve the catalytic properties of Pd: activated carbon[19, 44], TiO_2[37], Fe_3O_4[45], mesoporous zeolites[46], etc. In addition transition metal complexes can be considered as new active species or an intermediate of the active site [46-48].

The objectives of this work are: i) to synthesize different Pd-nanoparticle catalysts using a Pd(II) ammine complex as a precursor salt and supports of different acidity strength (γ-Al_2O_3, γ-Al_2O_3 modified with Mg and $CaCO_3$); ii) to evaluate the catalytic performances of the Pd-nanoparticle catalysts for purifying 1-pentene (a medium chain olefin) and the selective hydrogenation of long/medium chain terminal alkyne (C_7 and C_5) at mild reaction conditions; iii) to study the effects of the acidity (amount and strength), the type of active sites and the metal dispersion, on the catalytic activity and selectivity; iv) to compare the performance of the synthesized catalysts with that of a commercial Lindlar catalyst.

2. Experimental Section

2.1. Catalyst Preparation

Two inorganic materials, $CaCO_3$ (Anedra, purity 98.6%) and γ-Al_2O_3 (CK-300 powder, 35-80 meshes, calcined 3 h at 823 K in air) were used as supports. $CaCO_3$ was used without

previous treatment. A fraction of alumina was impregnated with an aqueous solution of $MgSO_4.7H_2O$ (Anedra, purity 99.8 %, 0.322 g $MgSO_4.7H_2O/g_{alumina}$) in order to obtain 5 wt% Mg. Then it was dried 24 h at 373 K and calcined for 3 h at 823 K, and was called Al_2O_3-Mg.

The colorless complex of $[Pd(NH_3)_4]Cl_2$ was prepared in a glass equipment under gentle stirring and reflux heating in a purified argon atmosphere. 0.5 g of $PdCl_2$ (Aldrich, purity 99%) and a solution of 55 mL of commercial NH_3 (Cicarelli, purity 30%) and 45 mL of NH_3/NH_4^+ buffer solution at pH = 10.5 were placed in the equipment and kept at 278 K for 4 h.

Pd/Al_2O_3, Pd/Al_2O_3–Mg and $Pd/CaCO_3$ catalysts were obtained by incipient wetness impregnation. Three successive impregnations of the aqueous solution of $[Pd(NH_3)_4]Cl_2$ were carried out on each support in order to obtain 0.4 wt% Pd with intermediate drying at room temperature. Then the synthetized monometallic catalysts were dried at 393 K for 24 h. The Al_2O_3 and Al_2O_3-Mg catalysts were calcined in air at 773 K for 3 h and the $[Pd(NH_3)_4]Cl_2/CaCO_3$ catalyst was calcined in a N_2 stream at 673 K for 3 h in order to stabilize palladium nanoparticles and prevent the decomposition of $CaCO_3$. Finally all catalysts were reduced 1 h with H_2 (573 K, 50 mL min^{-1}) in a tubular continuous flow quartz reactor.

2.2. Catalysts Characterization

A Micromeritics ASAP 2020 instrument was used to obtain the nitrogen adsorption-desorption isotherms at 0.02-0.98 (P/P_o) relative pressure. The BET model was used to calculate the specific surface area (S_{BET}) of the supports. Samples were first outgassed 2 h at 523 K in a vacuum and then N_2 adsorption isotherms at 77 K were obtained.

The mass content of Pd in the catalysts was determined by Atomic Emission Spectroscopy with Inductive Plasma (ICP-AES) with a Perkin Elmer OPTIMA 2120 equipment after digesting the samples in dilute sulfuric acid at 363 K.

The acid strength and the amount of acid sites on the surface of the solids were measured by temperature programmed desorption using pyridine as a probe molecule (TPD-Py). Measurements were made in a tubular reactor coupled to a Shimadzu GC-8A gas chromatograph with a FID detector. Before the analysis 200 mg of the samples were *ex situ* reduced at 573 K for 30 min. The solids were then calcined in N_2 (723 K, 40 mL min^{-1}) to desorb physisorbed compounds. The samples were then cooled down to room temperature and a nitrogen stream saturated with pyridine was allowed to flow over the sample for 30 min. Weakly physisorbed pyridine was then removed by stripping with nitrogen (418 K, 1 h, 40 mL min^{-1}). Then the temperature was increased from 418 up to 1000 K at a heating rate of 10 K min^{-1}. The gases issued by the reactor were directly sent to the methanator and analyzed with a flame ionization detector (FID). The signal of the detector was continuously recorded along with the sample temperature.

The electronic state of surface species was obtained by X-ray photoelectron spectroscopy (XPS). Ranges were chosen to inspect the Pd $3d_{5/2}$ and Ca $2p_{3/2}$ signals as well as the 2p signals of Mg, Cl and Al. The measurements were made in a VG-Microtech Multilab instrument equipped with a MgK_α source ($h\upsilon$: 1253.6 eV) and an energy of 50 eV. The pressure during data acquisition was maintained at 5.10^{-7} Pa. The samples were previously reduced 1 h at 573 K in flowing hydrogen, following the same pretreatment conditions of the reaction tests. The areas of the peaks were estimated by calculating the integral of each peak after subtracting a Shirley background and fitting the experimental peak to a combination of Lorentzian/Gaussian lines of

30–70% proportions. The reference signals were the Al 2p at 74.7 eV and the Ca $2p_{3/2}$ at 346.6 eV, corresponding to the Al_2O_3 and $CaCO_3$ supports.

The crystalline structure of the catalysts was defined in an X-ray Diffraction (XRD) Shimadzu XD-D1 equipment, with a CuK_α (λ = 1.5405 Å) in the range $10 < 2\theta < 85^\circ$ at a scanning speed of 1º min^{-1}. Samples powdered were reduced *ex situ* in H_2 stream.

The metal particle size distribution was obtained by TEM using a JEOL 100 CX II electron microscope with an acceleration voltage of 100 kV and 270000x magnification. The samples were prepared by grinding the pellets, suspending the particles in ethanol and then sonicating for 15 min. A drop of this suspension was placed on a 200 mesh copper grid with a Formvar film and observed. A set of digital images were taken in order to identify the phases and measure the particle diameters. Digital Micrograph software was used to obtain the particle size distributions.

The reducibility of the surface species was evaluated by temperature programmed reduction (H_2-TPR). The measurements were made in a Micromeritics Auto Chem II equipment equipped with a thermal conductivity detector. Before the analysis the samples were subjected to a pretreatment in Ar at 673 K for 30 min, and then they were cooled down to room temperature. The reduction procedure was carried out using a mixture of 5% H_2 in Ar at a flowrate of 30 mL min^{-1} and heating ramp of 10 K min^{-1} from room temperature to 1273 K.

2.3. Catalytic Tests

The catalysts were evaluated with the selective hydrogenation of 1-heptyne (Fluka, Cat. No. 51950, >98%), 1-pentyne (Aldrich, Cat. No. 627-19-0, >99%) and a mixture of 30/70 % $^{v}/_{v}$ 1-pentyne:1-pentene (Aldrich, Cat. No. 109-67-1, >98.5%) at mild conditions, 150 kPa and 303 K. In each run 50 mL of 2 % $^{v}/_{v}$ reactant diluted in toluene (Merck, Cat. No. TX0735-44, >99%)

were put in a stainless steel batch reactor coated with polytetrafluoroethylene (PTFE), with a reactant/Pd molar ratio of 1100. Stirring at 750 rpm was used in order to eliminate external diffusional limitations[49]. Reagents and products were analyzed by gas chromatography (GC) with a FID detector and an HP INNOWax capillary column of polyethyleneglycol (PEG). The Lindlar commercial catalyst (Aldrich, Cat. No. 20,573-7) was used for comparative purposes without any pretreatment as suggested by other authors for the hydrogenation of alkynes [50].

3. Results and Discussion

3.1. Catalysts Characterization

The nitrogen sortometry results are shown in Table 1. Surface area (S_{BET}), V_p (average pore volume) and d_p (average pore diameter) were calculated from N_2 physisorption isotherms for the three supports used: Al_2O_3, Al_2O_3-Mg and $CaCO_3$. All supports had different surface areas. Al_2O_3 displayed the largest BET area, while $CaCO_3$ had the lowest. The Al_2O_3 support modified with Mg (Al_2O_3-Mg) had a remarkable reduction of the surface area, attributed to the incorporation of magnesium on the surface of Al_2O_3. The textural properties varied in the same way, Al_2O_3 pore volume being much higher than the pore volume of Mg doped alumina. These results are important because they can give an idea of the exposed surface area of the supports and their interaction with the precursor metal complex. On the other hand, the average pore diameter, d_p, of $CaCO_3$ was 10% higher than the d_p of Al_2O_3. The d_p of Al_2O_3-Mg was 25% lower than the d_p of Al_2O_3. The relative pore diameter loss of Al_2O_3-Mg must be due to the preferential deposition of magnesium particles in pore mouths.

Table 1. Results of N_2 physisorption isotherms of supports

Support	S_{BET} ($m^2\ g^{-1}$)	V_p ($cm^3\ g^{-1}$)	d_p (nm)
Al_2O_3	180	0.53	9.6
Al_2O_3-Mg	120	0.22	7.2
$CaCO_3$	4	0.01	10.6

Results of temperature programmed desorption of pyridine of the supports (a) and the catalysts (b) are shown in Figure 1. The TPD traces had three desorption regions with different intensity. Region-I, located at low temperatures (400-600 K), Region-II at medium temperatures (600-760 K) and Region-III at high temperatures (760-1000 K). These regions correspond to sites of weak, moderate or strong acidity, respectively[51-53]. According to different authors[54, 55], the peaks of weak acidity can be attributed to Lewis acid sites, the peaks of moderate acidity to a combination of Lewis and Brönsted acid sites, while strong acid sites would be Brönsted sites. According to Figure 1.a the three supports had different types of acid sites. Al_2O_3 and Al_2O_3-Mg supports had two peaks of different intensities at high and low temperatures indicating the presence of both Lewis and Brönsted sites. In the case of $CaCO_3$, a single peak is seen at low temperature, indicating the sole presence of weak Lewis sites.

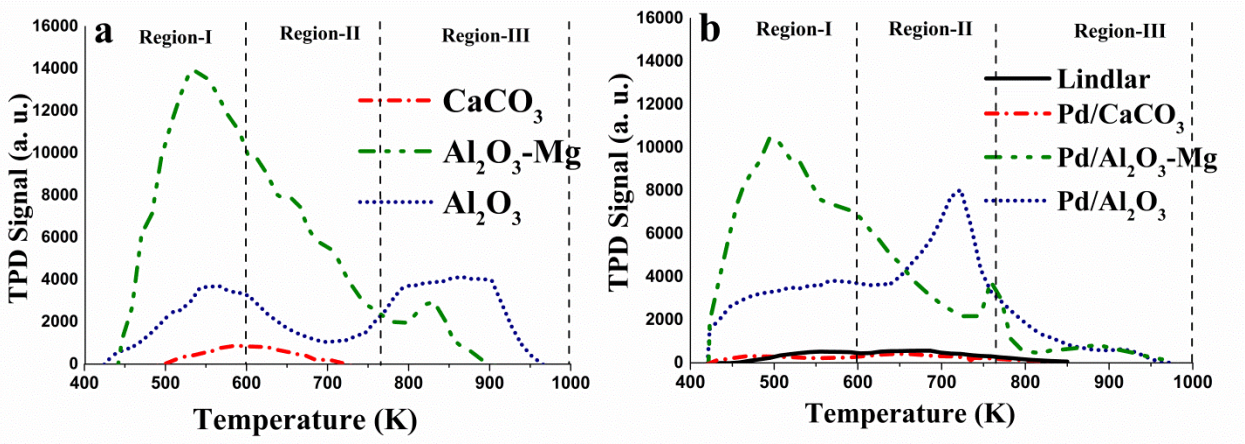

Figure 1. TPD-Py results. a) Supports. b) Catalysts.

Figure 1.b shows the TPD-Py traces of the Pd catalysts. It can be seen that the Pd/Al_2O_3 trace is very different from that of the Pd-free support, the area of Region-I increased markedly, a pronounced peak in the Region-II ca. 723 K appeared and the strong acidity peak of Region-III almost disappeared. Besides, the Pd/Al_2O_3-Mg TPD-Py trace was shifted to lower temperatures. $Pd/CaCO_3$ and Lindlar traces are quite similar to that of the Pd-free support.

The pyridine TPD traces were integrated to give the total amount of weak (400- 600 K), mild (600–760 K) and strong acid sites (T > 760 K). These acidity values were included in Table 2. Regarding the acidity values of the γ-Al_2O_3 fresh support, this had three kinds of acid sites, mainly strong (Brönsted). Al_2O_3-Mg support had the highest acidity, mainly attributed to the increase of the weak and medium acidity of Al_2O_3 (Lewis), while the strong acidity (Brönsted) was drastically reduced. This can be explained in Scheme 1 by the addition of Mg sulfate that produced two effects: (i) the transfer of a proton of the surface hydroxide groups (Brönsted acid sites) to the aqueous anion sulfate (Brönsted basic site); (ii) the bonding of aqueous Mg^{2+} (Lewis acid site) to the remnant surface oxidic site (Lewis basic site).

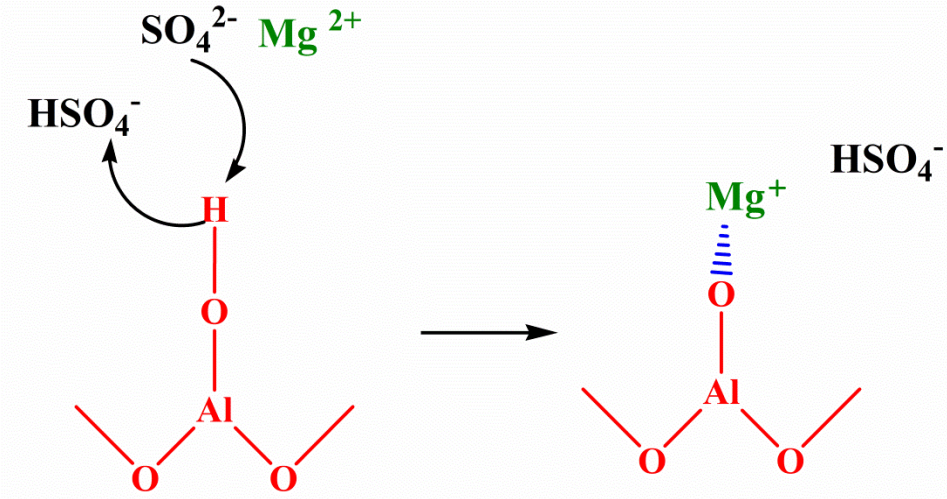

Scheme 1. Schematic drawing of simultaneous proton and ion-exchange on alumina Brönsted sites during $MgSO_4$ impregnation

The $CaCO_3$ support exhibited the lowest total acidity, only related to Ca^{2+} Lewis acid sites. This is related to the basic characteristics of this support, CO_3^{2-} being a soft basic Lewis site.

A marked increase in total acidity upon Pd addition is observed in Table 2. The observed order of total and weak acidity strength was: Pd/Al_2O_3-Mg >> Pd/Al_2O_3 >>> Lindlar > $Pd/CaCO_3$. The order of medium acidity strength was Pd/Al_2O_3 > Pd/Al_2O_3-Mg >>> Lindlar > $Pd/CaCO_3$. Total, medium and weak acidity of Lindlar and $Pd/CaCO_3$ were the lowest. This was mainly due to the basic character of the support. The TPD-Py profile of the Pd/Al_2O_3-Mg catalyst showed that the incorporation of Mg(II) and Pd(II) species over the alumina support, has the greatest effect on the quantity and quality of acidic properties, exhibiting greater weak acidity and higher total acidity, but a decrease of medium acidity in comparison to the Pd/Al_2O_3 catalyst. Feng et al[56, 57] showed a similar behavior in their studies using the TPD-NH_3 technique for a series of Pd-Mg based catalysts ($Pd/MgAl\text{-}LDH/Al_2O_3$, $PdO/MgO\text{-}Al_2O_3$, MgO modified Pd/Al_2O_3 and $Im\text{-}PdO/MgO\text{-}Al_2O_3$). The acidity increase was attributed to the presence of Pd

species, responsible for different types of Lewis acid sites and the loss of Brönsted sites of the catalysts. As shown in Scheme 2, during the synthesis of the catalysts, at pH ≅ 10.5, the Brönsted acid groups of the alumina or alumina modified supports would transfer the proton of the surface OH groups (Brönsted acid site) to the ammonia solvent (Brönsted basic site) and simultaneously the remnant oxidic site (Lewis basic Site) would bonds to Pd(II), a Lewis acid site, of the $[Pd(NH_3)_4]^{2+}$ complex. Previously, Brunelle[58] stated that at pH values below its IP (isoelectric point) an oxide particle adsorbs compensating anions like $[PdCl_4]^{2-}$, while at pH values above its IP, the surface acquires a net negative charge and adsorbs cations, like $[Pd(NH_3)_4]^{2+}$.

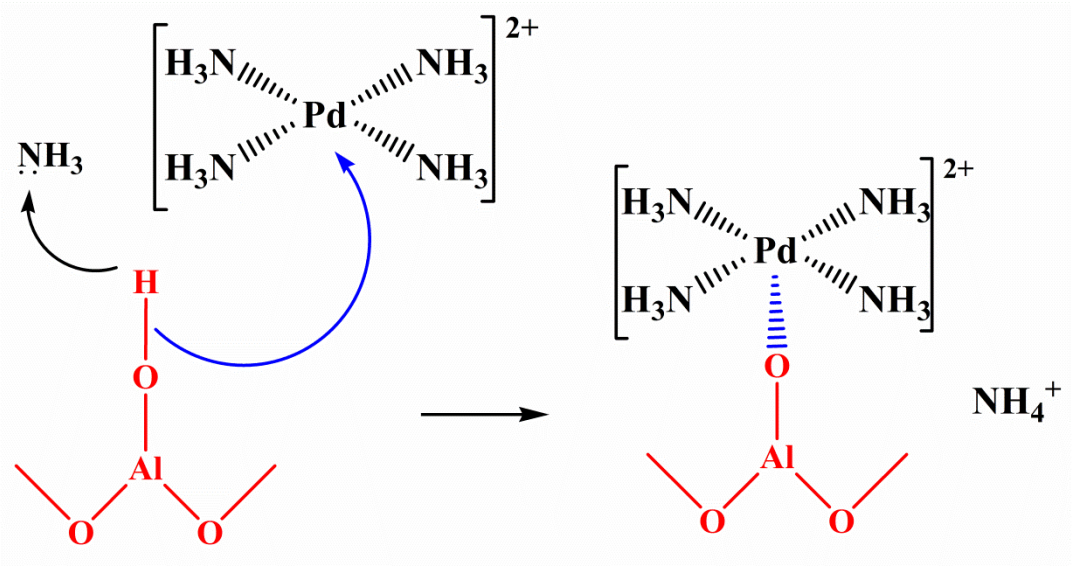

Scheme 2. Schematic drawing of simultaneous proton and ion-exchange on alumina free or modified during the impregnation of $[Pd(NH_3)_4]^{2+}$ in ammonia media.

Table 2. TPD-Py results.

Sample	Total Acidity ($\mu mol_{Py}\ g^{-1}$)	Weak Acidity ($\mu mol_{Py}\ g^{-1}$)	Medium Acidity ($\mu mol_{Py}\ g^{-1}$)	Strong Acidity ($\mu mol_{Py}\ g^{-1}$)
Al_2O_3	32.61	7.09	7.38	18.15
Al_2O_3-Mg	63.58	24.73	35.00	3.85
$CaCO_3$	1.00	1.00	--	---
Pd/Al_2O_3	56.76	18.72	37.82	0.22
Pd/Al_2O_3-Mg	72.92	53.31	19.32	0.29
Pd/$CaCO_3$	4.27	0.88	3.39	---
Lindlar	5.26	1.17	4.09	---

Results of characterization of the metal function by chemical analysis (ICP), XPS and TEM are shown in Table 3 for the Pd/Al_2O_3–Mg, Pd/$CaCO_3$ and Lindlar catalysts. The Lindlar catalyst had a very high Pd content, similar to that of commercial catalysts. In the case of the Pd/Al_2O_3 sample, the ICP analysis gave a Pd mass content very similar to the theoretical value. Slightly lower contents were found for the Pd/Al_2O_3–Mg and Pd/$CaCO_3$ catalysts. The presence of Mg was also confirmed by ICP analysis, as 5.5 wt% of Mg was detected during the preparation of the support.

Table 3. Metal loading as determined by ICP. Average particle size (d_{TEM}) and dispersion (D) from TEM microscopy. XPS results.

Sample	Pd (wt %)	d_{TEM} (nm)	D (%)	XPS				
				Pd $3d_{5/2}$ BE (eV)			Pd/S* ($\%^{at}/_{at}$)	Cl/Pd ($\%^{at}/_{at}$)
				Pd^{o}	$Pd^{\delta+}$	Pd^{n+}		
Pd/Al_2O_3	0.38	2.9	39	334.7 (62%)		336.3 (38%)	0.0016	2.09
Pd/Al_2O_3-Mg	0.30	3.0	37	334.9 (100%)		--	0.0063	0.95
$Pd/CaCO_3$	0.22	4.4	25	335.0 (100%)	--	--	0.022	5.14
Lindlar	5.00	46.0	2.5[35]	--	335.2 (69%)	336.9 (31%)	0.243	--

* Pd/S: atomic ratio Pd/Al for Pd/Al_2O_3 or Pd/Al_2O_3-Mg. Pd/Ca for $Pd/CaCO_3$ and Lindlar.

Figure 2 shows the TEM images and particle size distribution of the catalysts. Table 3 gives the average particle size (d_{TEM}) as determined by TEM and according to Equation (I):

$$d_{TEM} = \frac{\sum n_i . d_i^3}{\sum n_i . d_i^2} \qquad \text{(Eq. I)}$$

Where n_i is the number of particles with particle size d_i.

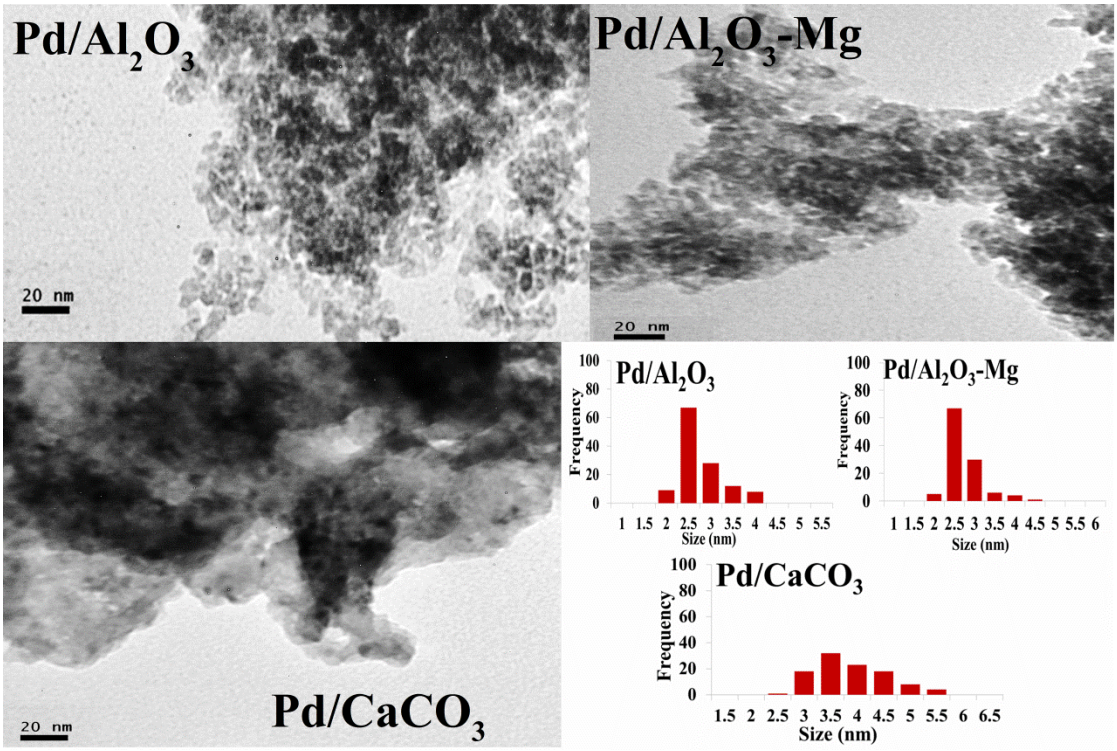

Figure 2. TEM images and particle size distribution of the catalysts.

The average particle sizes were very similar for Pd/Al_2O_3–Mg and Pd/Al_2O_3, 3.0 and 2.9 nm, respectively. This indicates that the incorporation of magnesium in the support does not significantly affect the particle size, mainly because of the low palladium loading. For the $Pd/CaCO_3$ catalyst the particle size is slightly higher: 4.4 nm. From these results, considering the spherical particle model adopted by Paryjczak and Szymura[59] and using ρ_{Pd}= 1.202 10^7 g_{Pd} m^{-3}; σ_{Pd} = 1.27 10^{19} at_{Pd} m^{-2}, the metal dispersions D were calculated and presented in Table 3. In Pd/Al_2O_3–Mg and Pd/Al_2O_3 a very similar dispersion of metal active sites is observed on both supports (~39%), while for the $Pd/CaCO_3$ catalyst a lower dispersion of 25% is obtained. These results may be indicative of greater interaction of the precursor complex with the Al_2O_3 and Al_2O_3–Mg supports during wet impregnation due to its more acidic characteristics (Table 2) and similar specific surface area, as explained previously. It is also possible that the small pore

volume of the $CaCO_3$ support (see Table 1) favors a lower final dispersion because of palladium preferential deposition in pore mouths, thus blocking the pore structure.

The commercial Lindlar catalyst has a quite high average particle size (46 nm) and a lower dispersion (2.5%) than the prepared catalysts (Table 3). This can be attributed to a high amount of Pd having been deposited on a support of low area and acidity, thus promoting a greater agglomeration of the particles in the pore mouths.

Figure 3 shows the TPR traces of the prepared catalysts. The reduction of species at temperatures below 250 K cannot be observed due to equipment limitations. The $Pd/CaCO_3$, Pd/Al_2O_3 and Pd/Al_2O_3–Mg catalysts exhibited an initial reduction peak at 260, 285 and 299 K, respectively. This peak at low temperatures is assigned to the reduction of bulk PdO species to metallic palladium[60]; indicating that palladium is at least partly in the Pd° metal state after the reduction treatment before the catalytic tests. For these peaks, a shift to higher temperatures is observed in this order: $Pd/CaCO_3$ < Pd/Al_2O_3 < Pd/Al_2O_3–Mg which could indicate higher interaction forces between the metallic species with the support, consistent with the amount of weak acidity (related to Lewis sites). Figure 3 also shows that during TPR analysis, $Pd/CaCO_3$, Pd/Al_2O_3 and Pd/Al_2O_3-Mg had a negative peak at 266, 325 and 340 K, respectively[60], due to the release of hydrogen from the decomposition of the β-phase of Pd hydrides (β-HPd) formed during the reduction of PdO at low temperatures[60]. These species interact weakly with the support and therefore Pd can be easily reduced.

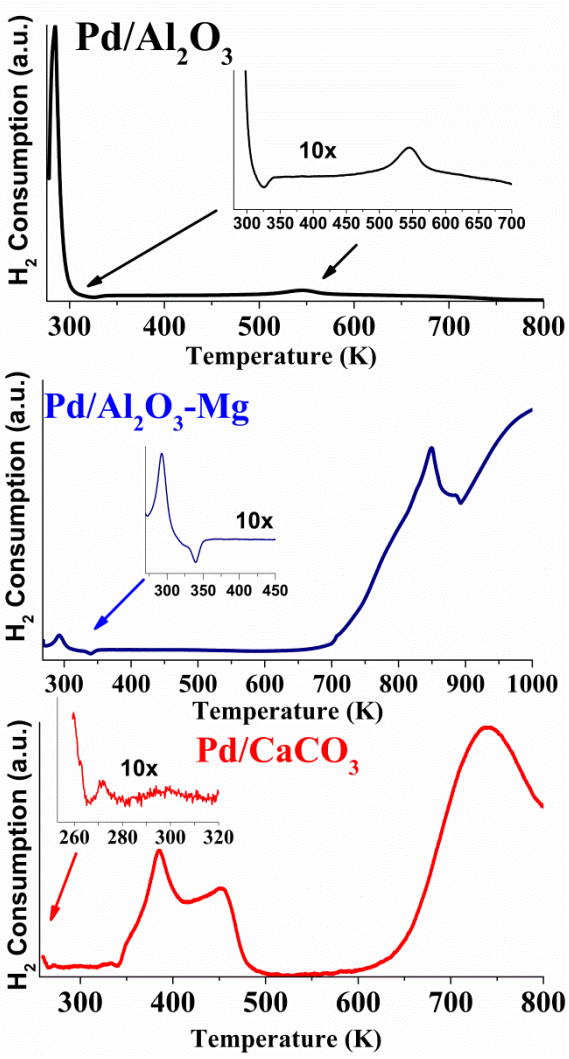

Figure 3. H_2-TPR traces of Pd/Al_2O_3, Pd/Al_2O_3–Mg and $Pd/CaCO_3$.

In Figure 3, medium intensity peaks at 385 and 451 K, and a very weak peak around 543 K are also observed on $Pd/CaCO_3$ and Pd/Al_2O_3 samples, respectively. Some authors suggest that the hydrogen consumption at these temperatures is due to the reduction of $Pd_xO_yCl_z$ oxychlorinated species or the reduction of Pd^{2+} ions stabilized by adjacent Cl^- remaining after the calcination process[61]. For Pd/Al_2O_3-Mg two extremely large peaks are observed in Figure 3 at temperatures higher than 700 K. They are both attributed to the reduction of the remaining sulfate magnesium precursor (SO_4^{2-}) that generates residual H_2S or SO_3 [62]. Additionally, in the

$Pd/CaCO_3$ sample, a wide peak between 633 and 800 K is seen that can be attributed to the decomposition of $CaCO_3$[63, 64].

Figure 4 shows the XPS spectra of the Pd *3d* region of Pd/Al_2O_3, Pd/Al_2O_3-Mg and $Pd/CaCO_3$ pretreated in hydrogen at 573 K, showing the Pd $3d_{5/2}$ and $3d_{3/2}$ signals separated by approximately 5 eV, in accordance with literature values[65]. The points are the experimental data and the curves beneath are the corresponding deconvoluted peaks. Figure 4 also shows the XPS spectrum of the Mg *2p* region of Pd/Al_2O_3-Mg. The Pd *3d* and Pb *4f* signals of the classical Lindlar catalyst [34] are also presented for comparative purposes. The deconvolution of the Pd $3d_{5/2}$ spectrum resulted in two peaks for the Pd/Al_2O_3 and Lindlar samples, indicating the presence of two different species of Pd on the catalysts. Pd/Al_2O_3-Mg and $Pd/CaCO_3$ spectra had one peak in the Pd $3d_{5/2}$ region, confirming the presence of single Pd species. These results are detailed in Table 3. The Pd/Al_2O_3 catalyst presents two BE peaks for Pd $3d_{5/2}$ at 334.7 (62 % $^{at}/_{at}$) and 336.3 eV (38% $^{at}/_{at}$), which are assigned to Pd° and Pd^{n+} (with *n* close to 2) electrodeficient oxychlorinated species formed during the calcination pretreatment [61]. The deconvolution of the Pd $3d_{5/2}$ signal for the Lindlar catalyst indicates two peaks at 335.2 eV (69 % $^{at}/_{at}$) and 336.9 eV (31 % $^{at}/_{at}$), assigned to $Pd^{\delta+}$ (with δ close to 0) and electrodeficient Pd^{n+} species (with *n* close to 2)[34, 66]. The deconvolution of the Pb $4f_{7/2}$ spectrum for the Lindlar catalyst shows two peaks at 136.8 eV (20% $^{at}/_{at}$) and 138.6 (80% $^{at}/_{at}$), attributed to Pb° and $Pb(OAc)_2$, respectively[34, 66]. In the case of the Pd/Al_2O_3–Mg and $Pd/CaCO_3$ catalysts the palladium signal is observed at a BE of 334.9 and 335.0 eV (100 % $^{at}/_{at}$), respectively, indicating the presence of the totally reduced Pd° at surface level, according to the literature [66]. In the Pd/Al_2O_3–Mg catalyst the BE of the Mg *2p* signal was located at 51.6 eV and was attributed to MgO surface species[66] seemingly confirmed by the ICP analysis. Deconvolution of the XPS spectra of the Pd prepared catalysts also showed

a peak at ca. 198.5 eV that corresponds to Cl $2p_{3/2}$. This was associated to surface chloride species[66] not complete eliminated after reduction.

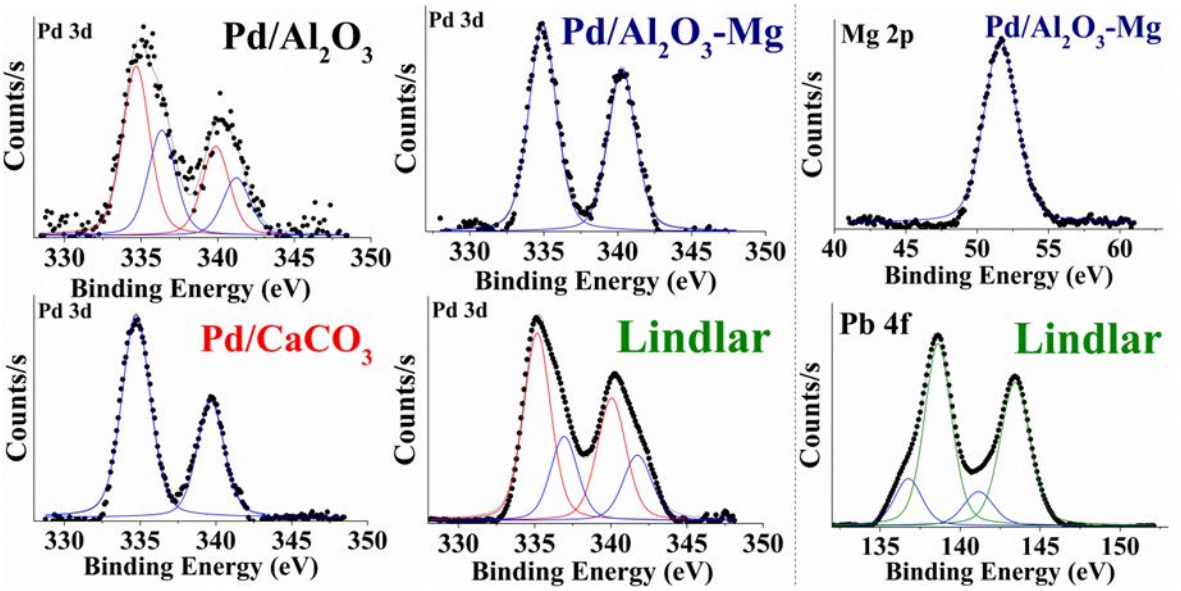

Figure 4. XPS spectra of the Pd *3d* region of all catalysts. Mg *2p* of Pd/Al_2O_3-Mg. Pb *4f* of the Lindlar[34] catalyst.

Values of the superficial Pd/S (Pd/Al for Pd/Al_2O_3 and Pd/Al_2O_3-Mg; Pd/Ca for $Pd/CaCO_3$ and Lindlar) and Cl/Pd (% $^{at}/_{at}$) atomic ratios are also shown in Table 3. With respect to the Pd/S atomic ratios as determined by XPS it is evident that the Pd/Al ratio is ca. 4 times higher for Pd/Al_2O_3–Mg in comparison to Pd/Al_2O_3 (0.0063 and 0.0016, respectively). For the $Pd/CaCO_3$ and Lindlar catalyst the Pd/Ca atomic ratio was the highest (0.022 and 0.243). This could be related to the differences in BET area and the very low pore volume (V_p) that favor a high content of surface palladium. Cl/Pd atomic ratios decrease in the following order: $Pd/CaCO_3$>> Pd/Al_2O_3 > Pd/Al_2O_3–Mg. The residual chlorine content in the catalysts after reduction could be explained by the different superficial adsorption capacities of each support. The presence of Cl^-

may also have some influence on the metallic dispersion, as well as on the performance of the catalysts.

According to XPS and TPR, the reduction pretreatment (1 h, 573 K, hydrogen) would produce different surface species on each catalyst. Pd° on $Pd/CaCO_3$ and Pd/Al_2O_3–Mg. Pd° and Pd^{n+} on Pd/Al_2O_3. $Pd^{\delta+}$ and Pd^{n+} on the Lindlar catalyst.

Figure 5 shows the XRD diffractograms of the catalysts and their corresponding database references (Pd, $CaCO_3$ and Al_2O_3). For the Pd/Al_2O_3–Mg and Pd/Al_2O_3 samples the presence of γ-alumina characteristic peaks at maximum intensity 2θ=37.7°, 45.9° and 66.9° is seen. $Pd/CaCO_3$ presents the characteristic peaks of the calcium carbonate, the main one being located at 2θ=29.4°. Due to the low concentration of Pd in all the samples (< 0.4 wt%), well below the detection limit of the XRD technique (> 5 wt%), the characteristic peaks of Pd(111) at 2θ= 40.1°, 46.7° and 68.2° were overlapped with the peaks of the supports and the presence of Pd crystallites was undetectable. On the Pd/Al_2O_3–Mg sample, the presence of $MgSO_4$ precursor residues was not detected because the characteristic peaks at 2θ =24° and 27° were absent. For the Lindlar catalyst the characteristic peak of Pd(111) is observed at 2θ= 40.1°. In spite of the very high Pd load (5 wt%) the pattern is dominated by strong and narrow reflexes of the $CaCO_3$ support. This is consistent with data previously reported by Tripathi et al[67].

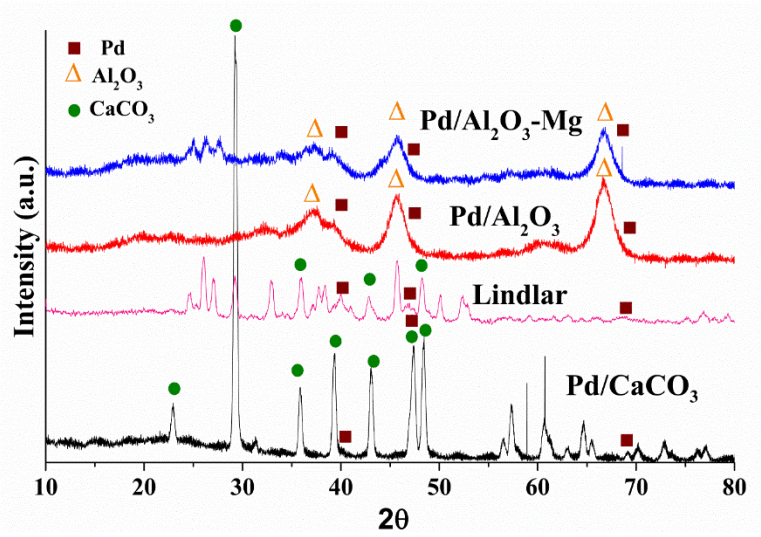

Figure 5. X-ray diffractograms of the catalysts.

3.2. Catalytic Test

The previous characterization analysis will allow us to correlate the properties of the synthesized catalysts with the activity and selectivity during the purification of a medium-chain olefin and during the hydrogenation of pure alkynes under mild operating conditions. The obtained results are compared with the Lindlar commercial catalyst at identical working conditions.

3.2.1. Hydrogenation of Pure 1-Heptyne and 1-Pentyne

Figure 6.a shows the results of total conversion of 1-heptyne (X) as a function of time and Figure 6.b shows the selectivity to 1-heptene (S) as a function of total conversion. It can be seen that all the catalysts are active and selective at mild operational conditions, 150 kPa and 303 K. Pd/Al_2O_3 has a very high 1-heptyne total conversion, while Pd/Al_2O_3–Mg, $Pd/CaCO_3$ and Lindlar present very similar total conversion values, being slightly higher for Pd/Al_2O_3–Mg. All catalysts had high selectivity to 1-heptene (> 80%), comparable to that of the Lindlar commercial

one. Initially and up to X=30% the selectivity of Pd/Al_2O_3 was the highest (≥ 95%). Between X=30 - 80% the selectivity begins to decrease, reaching 70% for X=99.9%. For X higher than 20% the selectivity of the Lindlar catalyst (S=82%) was lower than the selectivity of Pd/Al_2O_3–Mg (S=90%) and $Pd/CaCO_3$. This was particularly the case at X values higher than 90%. These results show a better performance of all the synthesized catalysts in comparison to the Lindlar commercial one, or to other catalysts previously reported [19] for the selective hydrogenation of 1-heptyne. Lederhos et al.[19] evaluated Pd, Pt and Ru catalysts supported on an activated carbon (RX3, Norit) during the selective hydrogenation of 1-heptyne at the same conditions of this work: 303 K and 150 kPa. Pd catalysts prepared with different precursor salts, $PdCl_2$ or $Pd(NO_3)_2$, were the most active and selective, reaching a total conversion of 1-heptyne at 120-180 min with 85-90% selectivity. In the case of the PdClRX catalyst the authors observed that from a total conversion of ca. 80% the selectivity to 1-heptene decreased sharply while PdNRX had a constant selectivity of 87%. The differences in activity and selectivity between PdClRX and PdNRX were attributed to several factors: a better accessibility of the alkyne to the active sites, thermodynamic factors, and electronic or steric effects of the surface groups on the activated carbon support[19].

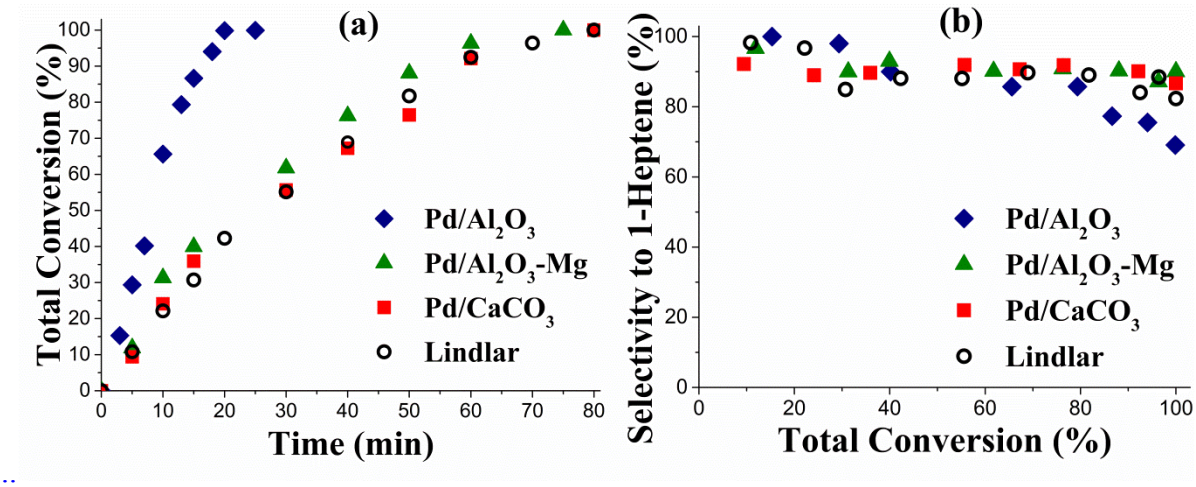

Figure 6. (a) Total Conversion of 1-Heptyne (%) vs. Time (min) and (b) Selectivity to 1-Heptene (%) vs. Total Conversion (%) for Pd/Al_2O_3 (♦), Pd/Al_2O_3–Mg (▲), $Pd/CaCO_3$ (■) and Lindlar (○).

Figure 7.a shows results of total conversion as a function of time and Figure 7.b values of selectivity to 1-pentene as a function of total conversion during the hydrogenation of 1-pentyne. The following order of 1-pentyne total conversion can be found in Figure 7.a: Pd/Al_2O_3 >> Pd/Al_2O_3–Mg > Lindlar >> $Pd/CaCO_3$. A comparison of Figures 6.a and 7.a shows that in all cases the hydrogenation reaction rates of 1-pentyne are greater than those of 1-heptyne. Regarding the selectivity to 1-pentene in Figure 7.b, all synthesized catalysts have very high selectivity to 1-pentene, ca. 90%, very similar to that obtained using the Lindlar commercial catalyst.

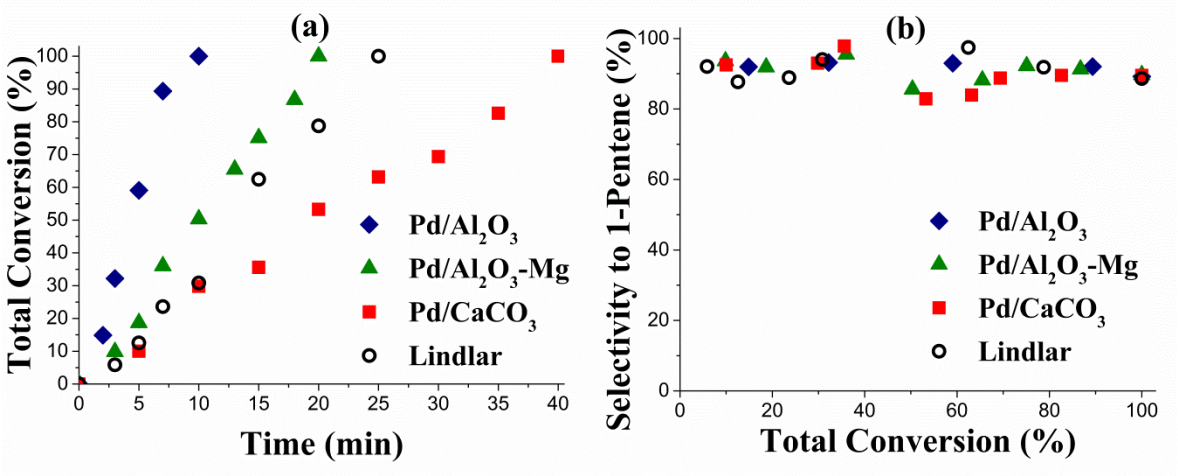

Figure 7. (a) Total Conversion of 1-Pentyne (%) vs. Time (min) and (b) Selectivity to 1-Pentene (%) vs. Total Conversion (%) for Pd/Al_2O_3 (♦), Pd/Al_2O_3–Mg (▲), $Pd/CaCO_3$ (■) and Lindlar (○).

Table 4 contains values of selectivity at the end of the run at isoconversion conditions (X≈99.9 %) and values of the initial reaction rate (mass based r^0 and TOF) for all catalysts compared and for the different feeds used. TOF values were calculated using initial reaction rates of alkyne calculated from the data plotted in Figures 6.a and 7.a and dispersion values indicated in Table 3. The initial reaction rate of the alkynes was calculated using the following formula:

$$r^0 = \frac{V.C^0}{W_{Pd}} \cdot \left(\frac{\partial X}{\partial t} \right)_{t=0} \qquad \text{Ec. (II)}$$

r^0 is the initial reaction rate of the alkyne [mol g_{Pd}^{-1} min^{-1}]. $(\partial X/\partial t)_{t=0}$ is the tangent value of the plot of alkyne total conversion versus time at t = 0a. C^0 is the initial concentration of alkyne [mol L^{-1}], W_{Pd} the mass of palladium [g_{Pd}], V the reaction volume [L] and t the reaction time [min].

Table 4. Comparison of catalytic results.

Catalyst	Reactant	t (min)	X (%)	S* (%)	r^0 (mol $g_{Pd}^{-1}min^{-1}$)	TOF (min^{-1})
Pd/Al_2O_3	1-Heptyne	20	99.9	70	76.20	2.03
Pd/Al_2O_3-Mg	1-Heptyne	75	99.9	90	33.18	0.90
$Pd/CaCO_3$	1-Heptyne	80	99.9	87	32.41	1.33
Lindlar	1-Heptyne	80	99.9	82	28.61	12.18
Pd/Al_2O_3	1-Pentyne	10	99.9	86	155.65	4.14
Pd/Al_2O_3-Mg	1-Pentyne	20	99.9	90	53.17	1.45
$Pd/CaCO_3$	1-Pentyne	40	99.9	90	37.11	1.52
Lindlar	1-Pentyne	25	99.9	89	35.97	15.31
Pd/Al_2O_3	1-Pentyne/1-Pentene	18	99.9	91	186.64	4.97
Pd/Al_2O_3-Mg	1-Pentyne/1-Pentene	50	99.9	93	41.11	1.12
$Pd/CaCO_3$	1-Pentyne/1-Pentene	140	93.0	89	32.31	1.32
Lindlar	1-Pentyne/1-Pentene	30	99.9	88	38.72	16.48

*Selectivity to the corresponding alkene product.

For the hydrogenation of the pure alkynes, the following initial reaction rate order is found: Pd/Al_2O_3 >> Pd/Al_2O_3–Mg ≥ $Pd/CaCO_3$ > Lindlar. Besides its high activity it is important to note that Pd/Al_2O_3 has the lowest selectivity to 1-heptene and 1-pentene, while the other catalysts have high selectivity to the desired alkene product, quite similar to that obtained with the Lindlar commercial catalyst. Therefore on the basis of activity and selectivity all the prepared catalysts were comparable or better than the Lindlar catalyst for hydrogenation of alkynes. The activity and selectivity results suggest a better synergism between the Pd nanoparticles and the supports, probably because of an easier dissociation of hydrogen over the metal center, as reported by Jackson et al.[32] In these reaction the initial reaction rate is supposed to be related to the dissociative adsorption of hydrogen[40]. It is well known that during hydrogenations metallic centers rich in electrons can cleave the H-H bond by means of the interaction of a filled ***d*** metal orbital with the empty σ antibonding molecular orbital of H_2 [68]. This scission is favored on Pd°

sites with a d^{10} configuration. The adsorption of H_2 would also be favored over small particles. As observed in Table 3 the Pd/Al_2O_3, Pd/Al_2O_3-Mg and-$Pd/CaCO_3$ catalysts show a high amount of Pd° active species and small particle sizes. The dissociative adsorption of hydrogen and the whole catalytic cycle would then be enhanced[69, 70].

The high activity of the Pd/Al_2O_3 catalyst can be explained by three main factors: a) electronic effects of Pd° species (with *3d* BE of 334.7 eV, as found by XPS) that can improve the dissociative cleavage of H-H due to a high d^{10} electron availability; b) Pd^{n+} electrodeficient species (acid Lewis sites) favoring the adsorption of the terminal alkyne via the alkyne triple bonds (basic Lewis sites); and c) remaining Brönsted acid sites of alumina providing additional protonic hydrogen. These factors would enhance the hydrogenation rate. Factors b) and c) would also favor overhydrogenation and isomerization undesirable reactions, thus decreasing the selectivity of the Pd/Al_2O_3 catalyst.

The Pd/Al_2O_3-Mg is also more active than the Lindlar catalyst. Again the presence of a high concentration of Pd° nanoparticles and Lewis acid sites ($MgO\text{-}Al_2O_3$ surface species) for adsorption of the alkyne, would explain this activity (electronic effect). The high selectivity could be related to geometrical or steric effects of cationic magnesium surface species inhibiting isomerization reactions. In turn the high selectivity of $Pd/CaCO_3$ could be assigned to the carbonate groups (soft Lewis base) preventing undesirable isomerization reactions (electronic effects). Finally the high selectivity of the Lindlar catalysts is attributed to the presence of surface lead species, which prevent isomerization reactions due to electronic effects.

It is important to note that the rate of hydrogenation of 1-pentyne is higher than that of 1-heptyne because the 1-pentyne molecule is smaller. It is less inhibited by surface groups by geometrical effects both for adsorption and hydrogenation of the triple bond. The larger terminal

alkyne can also be adsorbed either in a perpendicular or parallel way and this can hinder the interaction with the catalyst active centers[71, 72].

3.2.2. Purification of 1-pentene

As mentioned in the Introduction the selective hydrogenation of the triple bond (C≡C) of alkynes in the presence of a high concentration of alkenes (double bonds) is of great importance, and especially for the purification of C_5 olefinic streams, e.g. for production of polymers. In order to assess the performance in this situation, the prepared catalysts were evaluated in the reaction of purification of 1-pentene (1-pentyne/1-pentene feedstock, 30:70 % $^{v}/_{v}$) at mild reaction conditions (150 kPa and 303 K). The 1-alkyne total conversion and selectivity to 1-alkene of each catalyst were compared against those of the Lindlar commercial catalyst.

Figure 8 shows the 1-pentyne total conversion vs. time and selectivity to 1-pentene as a function of total conversion. Figure 9 shows the concentration of reactants and product as a function of time. As shown in both Figures all catalysts were active and selective for the purification of 1-pentene. Table 4 shows values of the 1-pentyne initial reaction rate (r^0, calculated using Eq. (II)) and the turnover frequency (TOF). The most active catalyst was Pd/Al_2O_3, followed by Pd/Al_2O_3-Mg and the Lindlar catalyst. The $Pd/CaCO_3$ catalyst was the least active. As shown in Figure 8 all the prepared catalysts had good selectivity to the desired product, 1-pentene, ca. 88-98%. Besides, the Pd/Al_2O_3 catalyst was the only one producing isomers. During the purification of alkenes, the alkyne efficiently blocks alkene re-adsorption, but some catalytic properties e.g.: acidity or particle sizes can have an influence on isomerization or overhydrogenation undesired, which are generated especially when a 30-10% of residual alkyne remains in the reactor. Small particle sizes of Pd° active sites and the presence of acid

Lewis sites (electronic effects) seem responsible for the high reaction rate of Pd/Al_2O_3 and Pd/Al_2O_3-Mg. The Brönsted acid sites of the catalyst (electronic effect) would directly promote the isomerization reactions on Pd/Al_2O_3. On the other hand weaker acid sites (electronic effect) favoring 1-pentene desorption would be responsible for the highest selectivity of Pd/Al_2O_3–Mg.

High dispersion was favored by the use of an ionic complex $[Pd(NH_3)_4]^{2+}$ at pH=10 for the impregnation. This allowed the stabilization of Pd particles over the Brönsted acid sites of the support and prevented their agglomeration. Quesada et al.[73] have demonstrated to a large extent the importance of using metallic complexes during the synthesis of catalysts for hydrogenation. In our case, the low load of the prepared Pd catalysts (0.4 wt %) as compared to the high load of the Lindlar catalyst (5 wt %) suggests the presence of a metal monolayer distribution in the prepared catalysts and a less efficient "stack" distribution in the case of the Lindlar catalyst. Electronic effects by surface Pb species would also modify the Pd active sites ($Pd^{\delta+}$ and Pd^{n+}).

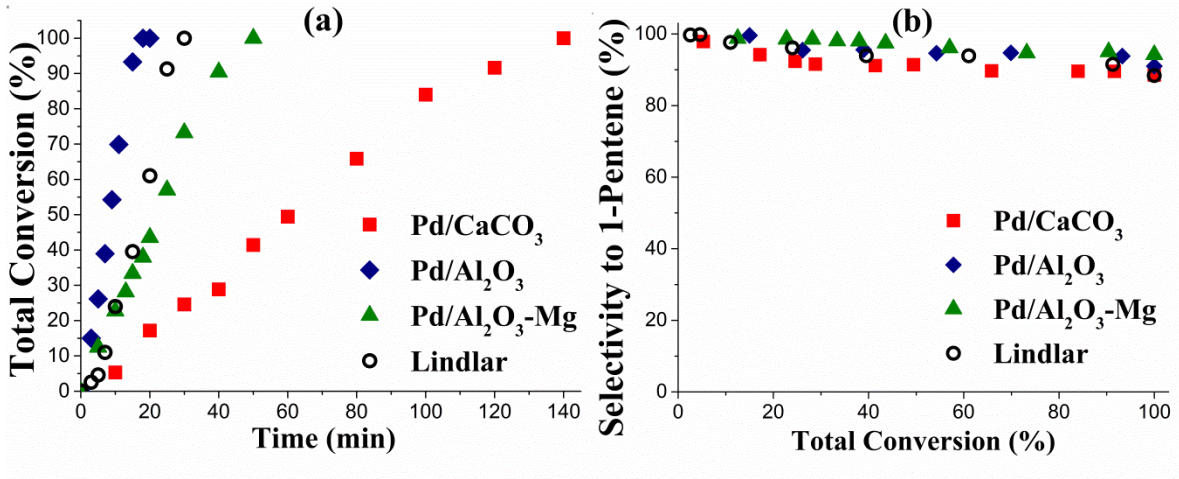

Figure 8. (a) Total Conversion of 1-Pentyne (%) vs. Time (min), and (b) Selectivity to 1-Pentene (%) vs. Total Conversion (%) during the hydrogenation of the 1-Pentyne/1-Pentene mixture (30:70 $\%^{v}/_{v}$), for Pd/Al_2O_3 (♦), Pd/Al_2O_3–Mg (▲), $Pd/CaCO_3$ (■) and Lindlar (○).

The XPS and TPR results helped understanding the properties and electronic effects in the prepared catalysts. The adsorption or interaction of unsaturated olefins can be rationalized by the effects of donation and acceptance of electrons involved in the bonds[72]. Metals such as Pd that have high H_2 chemisorption capacity are very much affected by the electronic effects of the supports[72]. XPS and TPR revealed that after the reduction of the catalysts with H_2 (1 h at 573 K) Pd° species were present on the surface. Pd° nanoparticles would favor the dissociative adsorption of hydrogen during the catalytic tests. The TPD-Py analysis also highlighted the differences of acidity of supports and catalysts (Table 2), the type of surface acidity having a great influence on the catalytic properties. The Pd/Al_2O_3 catalyst, with the highest distribution of medium acidity strength, had the highest 1-pentyne initial reaction rate, but it was the least selective, forming too much of branched alkenes. As previously stated the remaining Brönsted acid sites on alumina provide additional protonic hydrogen that increases the hydrogenation rate of 1-pentyne. These Brönsted acid sites are also responsible for the isomerization and overhydrogenation of 1-pentene. On the other side, Pd/Al_2O_3-Mg was the catalyst with the highest weak acidity, a high activity and the highest alkene selectivity. Totally reduced Pd° nanoparticles that favor H_2 dissociative chemisorption, and superficial cationic magnesium oxide species that favor alkyne chemisorption, would both be responsible for the high activity of the Pd/Al_2O_3-Mg catalyst. Its high selectivity can be explained by geometrical/steric effects of $MgO\text{-}Al_2O_3$ surface species that would prevent isomerization.

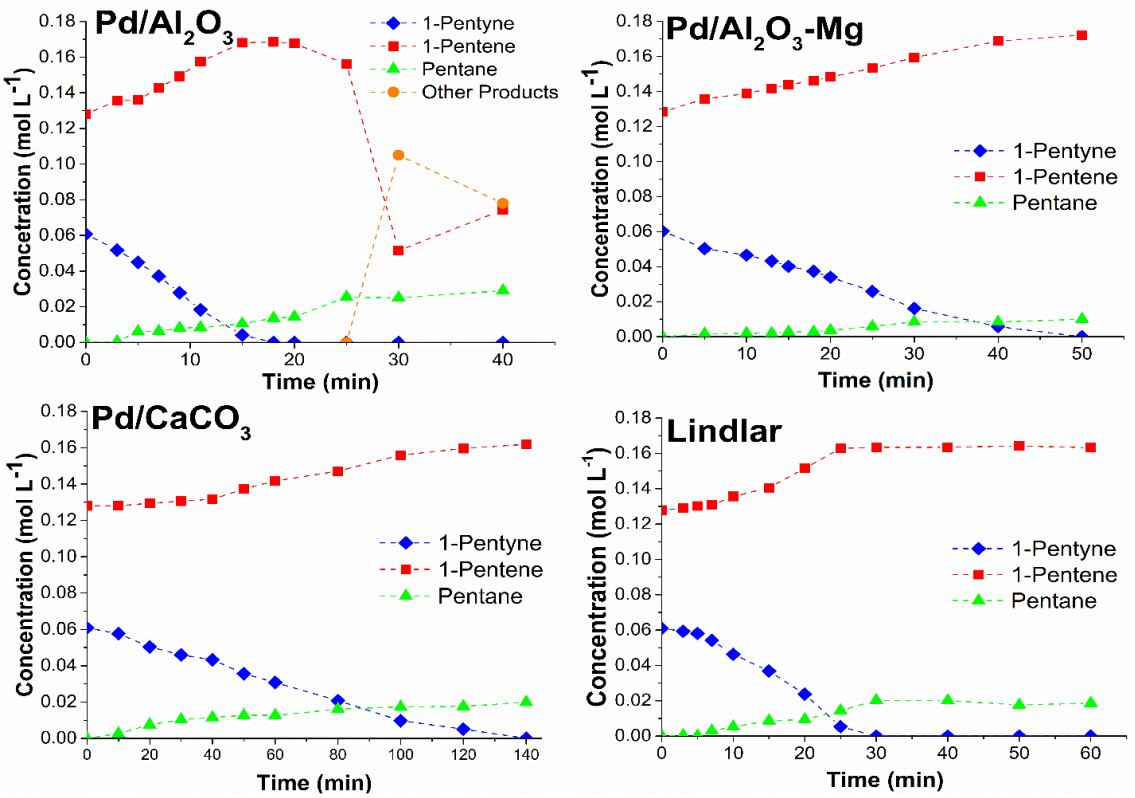

Figure 9. Concentration of reactants and products (mol L^{-1}) as a function of time (min). Hydrogenation of a 1-Pentyne/1-Pentene mixture (30:70 $^{v}/_{v}$).

$Pd/CaCO_3$ catalyst was an active and selective catalyst with significant results in the selective hydrogenation of alkynes; its activity and selectivity is comparable to that of Lindlar commercial catalyst. However its initial reaction rate was the lowest if compared to the Pd/Al_2O_3 or Pd/Al_2O_3-Mg catalysts. The lower activity can be partly attributed to its low acidity, with weak and medium acid sites being more abundant. This acid distribution could however be beneficial to the selectivity. Furthermore it should be noted that the presence of a big amount of Cl^- on the surface can induce electronic effects. Jackson et al [32] have indicated that residual chloride weakens the bond of surface terminal alkynes and decreases its reactivity. Badano et al. [61] have reported that the presence of Cl^- greatly improves the selectivity and resistance to sulfur

poisoning. Therefore the low initial reaction rate of $Pd/CaCO_3$ could be explained by two factors. First, by the low adsorption capacity of the carbonate support due to the weak electronic interaction between the surface calcium cationic species (hard Lewis acid) and the π electron of alkyne (soft Lewis base). Second, by the high surface concentration of electronegative chloride species that inhibits the adsorption of the alkyne (electronic effects). The high selectivity of $Pd/CaCO_3$ can be attributed to the presence of carbonate groups (soft Lewis base) that prevent the undesirable isomerization (electronic effect).

Taking into account the above results, on the basis of its high activity and selectivity (>90 %), the best catalyst for the purification of alkenes and/or the hydrogenation of pure terminal alkynes is the low loaded Pd/Al_2O_3-Mg. $Pd/CaCO_3$ is also a promising catalyst and could be the second choice, because it has a high selectivity (>89%), similar to that of the Lindlar catalyst (>88%).

4. Conclusions

Low-loaded Pd/Al_2O_3, Pd/Al_2O_3–Mg and $Pd/CaCO_3$ catalysts were prepared using chloride of tetraamminepalladium(II) as precursor solution. Highly dispersed Pd nanoparticles were obtained with an average particle size ca. 3-4.5 nm. These catalysts were evaluated with the purification of a C_5 olefin and with the selective hydrogenation of different medium chain terminal pure alkynes (C_7 and C_5). Lindlar commercial catalyst was used as reference.

The synthetized catalysts were characterized by ICP-AES, N_2 adsorption/desorption isotherm, TPD-Py, XRD, H_2-TPR, TEM and XPS.

TPD-Py results revealed different acidity distributions and suggested the adsorption of $[Pd(NH_3)_4]^{2+}$ over the Brönsted acid sites of alumina (Mg-free or Mg-doped) and over

superficial carbonate anions (Lewis base). The order of total acidity and weak acidity was the same: Pd/Al_2O_3-Mg >> Pd/Al_2O_3 >>> Lindlar > $Pd/CaCO_3$. Pd/Al_2O_3 had more mild acid sites.

XPS analysis revealed that all the prepared catalysts had a high concentration of Pd° nanoparticles.

The results of purification of 1-pentene and hydrogenation of 1-heptyne or 1-pentyne, at mild reaction conditions, showed that all the prepared catalysts were very active and highly selective to the 1–alkene product. Selectivity values were indeed higher than those of the Lindlar commercial catalyst.

Pd/Al_2O_3 was the most active but the least selective catalyst. This was attributed to Brönsted acid sites of medium strength providing additional protonic hydrogen, positively increasing the hydrogenation rate of 1-alkyne but negatively promoting the isomerization and over-hydrogenation of the terminal alkene. Pd/Al_2O_3-Mg, showed a high activity and the highest selectivity to the corresponding alkene. This was attributed to the presence of Pd° nanoparticles promoting the dissociative adsorption of hydrogen and surface $MgO\text{-}Al_2O_3$ species promoting the adsorption of the alkyne (electronic effects) and preventing isomerization (geometrical/steric effects).

Low-loaded Pd/Al_2O_3–Mg and $Pd/CaCO_3$ catalysts can be used for the purification of medium or large terminal alkenes at mild reaction conditions as an alternative to the high loaded Lindlar commercial catalyst.

Acknowledgment

The financial support provided by UNL (Grants CAI+D 50420150100074LI and 50420150100028LI), CONICET (Grant PIP 11220130100457CO) and ANPCyT (Grant PICT

2016 1453) are acknowledged.

References

1. Dobson, N. A.; Eglinton, G.; Krishnamurti, M.; Raphael, R. A.; Willis, R. G., Selective catalytic hydrogenation of acetylenes. *Tetrahedron* **1961,** *16* (1), 16-24.
2. Thomas, S. P.; Greenhalgh, M. D., 8.16 Heterogeneous Hydrogenation of CC and CC Bonds A2 - Knochel, Paul. In *Comprehensive Organic Synthesis II (Second Edition)*, Elsevier: Amsterdam, 2014; pp 564-604.
3. Carey, F. A.; Sundberg, R. J., *Advanced Organic Chemistry*. Springer US: 2000.
4. Lebel, H.; Paquet, V., Multicatalytic Processes Using Diverse Transition Metals for the Synthesis of Alkenes. *Journal of the American Chemical Society* **2004,** *126* (36), 11152-11153.
5. Sadrameli, S. M., Thermal/catalytic cracking of hydrocarbons for the production of olefins: A state-of-the-art review I: Thermal cracking review. *Fuel* **2015,** *140*, 102-115.
6. McCue, A. J.; Guerrero-Ruiz, A.; Ramirez-Barria, C.; Rodríguez-Ramos, I.; Anderson, J. A., Selective hydrogenation of mixed alkyne/alkene streams at elevated pressure over a palladium sulfide catalyst. *Journal of Catalysis* **2017,** *355* (Supplement C), 40-52.
7. Ji, Y.; Yang, H.; Yan, W., Catalytic cracking of n-hexane to light alkene over ZSM-5 zeolite: Influence of hierarchical porosity and acid property. *Molecular Catalysis* **2018,** *448*, 91-99.
8. Ramsurn, H.; Gupta, R. B., Chapter 15 - Hydrogenation by Nanoparticle Catalysts A2 - Suib, Steven L. In *New and Future Developments in Catalysis*, Elsevier: Amsterdam, 2013; pp 347-374.
9. Blaser, H.-U.; Schnyder, A.; Steiner, H.; Rössler, F.; Baumeister, P., Selective Hydrogenation of Functionalized Hydrocarbons. In *Handbook of Heterogeneous Catalysis*, Wiley-VCH Verlag GmbH & Co. KGaA: 2008.
10. Chen, B.; Dingerdissen, U.; Krauter, J. G. E.; Lansink Rotgerink, H. G. J.; Möbus, K.; Ostgard, D. J.; Panster, P.; Riermeier, T. H.; Seebald, S.; Tacke, T.; Trauthwein, H., New developments in hydrogenation catalysis particularly in synthesis of fine and intermediate chemicals. *Applied Catalysis A: General* **2005,** *280* (1), 17-46.
11. Segura, Y.; López, N.; Pérez-Ramírez, J., Origin of the superior hydrogenation selectivity of gold nanoparticles in alkyne + alkene mixtures: Triple- versus double-bond activation. *Journal of Catalysis* **2007,** *247* (2), 383-386.
12. McCue, A. J.; Gibson, A.; Anderson, J. A., Palladium assisted copper/alumina catalysts for the selective hydrogenation of propyne, propadiene and propene mixed feeds. *Chemical Engineering Journal* **2016,** *285* (Supplement C), 384-391.
13. Lopez, N.; Vargas-Fuentes, C., Promoters in the hydrogenation of alkynes in mixtures: insights from density functional theory. *Chemical Communications* **2012,** *48* (10), 1379-1391.
14. Insorn, P.; Kitiyanan, B., Selective hydrogenation of mixed C4 containing high vinyl acetylene by Mn-Pd, Ni-Pd and Ag-Pd on Al2O3 catalysts. *Catalysis Today* **2015,** *256*, 223-230.
15. Bazzazzadegan, H.; Kazemeini, M.; Rashidi, A. M., A high performance multi-walled carbon nanotube-supported palladium catalyst in selective hydrogenation of acetylene-ethylene mixtures. *Applied Catalysis A: General* **2011,** *399* (1), 184-190.

16. Benavidez, A. D.; Burton, P. D.; Nogales, J. L.; Jenkins, A. R.; Ivanov, S. A.; Miller, J. T.; Karim, A. M.; Datye, A. K., Improved selectivity of carbon-supported palladium catalysts for the hydrogenation of acetylene in excess ethylene. *Applied Catalysis A: General* **2014,** *482*, 108-115.
17. Ibhadon AO , K. S., The Reduction of Alkynes Over Pd-Based Catalyst Materials- A Pathway to Chemical Synthesis. *Journal of Chemical Engineering & Process Technology* **2018,** *9* (2), 376.
18. Tew, M. W.; Janousch, M.; Huthwelker, T.; van Bokhoven, J. A., The roles of carbide and hydride in oxide-supported palladium nanoparticles for alkyne hydrogenation. *Journal of Catalysis* **2011,** *283* (1), 45-54.
19. Lederhos, C. R.; Badano, J. M.; Carrara, N.; Coloma-Pascual, F.; Almansa, M. C.; Liprandi, D.; Quiroga, M., Metal and Precursor Effect during 1-Heptyne Selective Hydrogenation Using an Activated Carbon as Support. *The Scientific World Journal* **2013,** *2013*, 9.
20. Nikoshvili, L. Z.; Makarova, A. S.; Lyubimova, N. A.; Bykov, A. V.; Sidorov, A. I.; Tyamina, I. Y.; Matveeva, V. G.; Sulman, E. M., Kinetic study of selective hydrogenation of 2-methyl-3-butyn-2-ol over Pd-containing hypercrosslinked polystyrene. *Catalysis Today* **2015,** *256*, 231-240.
21. Werner Bonrath, J. M., Jan Schütz,; Bettina Wüstenberg, T. N., Hydrogenation in the Vitamins and Fine Chemicals Industry – An Overview. *InTech,* **2012,** *Hydrogenation.*, 66-90.
22. Al-Herz, M.; Simmons, M. J. H.; Wood, J., Selective Hydrogenation of 1-Heptyne in a Mini Trickle Bed Reactor. *Industrial & Engineering Chemistry Research* **2012,** *51* (26), 8815-8825.
23. Kittisakmontree, P.; Yoshida, H.; Fujita, S.-i.; Arai, M.; Panpranot, J., The effect of TiO2 particle size on the characteristics of Au–Pd/TiO2 catalysts. *Catalysis Communications* **2015,** *58*, 70-75.
24. Garcia, P. E.; Lynch, A. S.; Monaghan, A.; Jackson, S. D., Using modifiers to specify stereochemistry and enhance selectivity and activity in palladium-catalysed, liquid phase hydrogenation of alkynes. *Catalysis Today* **2011,** *164* (1), 548-551.
25. Nijhuis, T. A.; van Koten, G.; Moulijn, J. A., Optimized palladium catalyst systems for the selective liquid-phase hydrogenation of functionalyzed alkynes. *Applied Catalysis A: General* **2003,** *238* (2), 259-271.
26. Crespo-Quesada, M.; Yarulin, A.; Jin, M.; Xia, Y.; Kiwi-Minsker, L., Structure Sensitivity of Alkynol Hydrogenation on Shape- and Size-Controlled Palladium Nanocrystals: Which Sites Are Most Active and Selective? *Journal of the American Chemical Society* **2011,** *133* (32), 12787-12794.
27. Hu, J.; Zhou, Z.; Zhang, R.; Li, L.; Cheng, Z., Selective hydrogenation of phenylacetylene over a nano-Pd/α-Al2O3 catalyst. *Journal of Molecular Catalysis A: Chemical* **2014,** *381*, 61-69.
28. Mastalir, Á.; Király, Z.; Szöllösi, G.; Bartók, M., Stereoselective hydrogenation of 1-phenyl-1-pentyne over low-loaded Pd-montmorillonite catalysts. *Applied Catalysis A: General* **2001,** *213* (1), 133-140.
29. Canning, A. S.; Jackson, S. D.; Monaghan, A.; Wright, T., C-5 alkene hydrogenation: Effect of competitive reactions on activity and selectivity. *Catalysis Today* **2006,** *116* (1), 22-29.
30. Hamilton, C. A.; Jackson, S. D.; Kelly, G. J.; Spence, R.; de Bruin, D., Competitive reactions in alkyne hydrogenation. *Applied Catalysis A: General* **2002,** *237* (1), 201-209.

31. Jackson, S. D.; Shaw, L. A., The liquid-phase hydrogenation of phenyl acetylene and styrene on a palladium/carbon catalyst. *Applied Catalysis A: General* **1996,** *134* (1), 91-99.
32. Jackson, S. D.; Hamilton, C. A.; Kelly, G. J.; de Bruin, D., The Hydrogenation of c-5 Alkynes over Palladium Catalysts. *Reaction Kinetics and Catalysis Letters* **2001,** *73* (1), 77-82.
33. Murugesan, K.; Alshammari, A. S.; Sohail, M.; Beller, M.; Jagadeesh, R. V., Monodisperse nickel-nanoparticles for stereo- and chemoselective hydrogenation of alkynes to alkenes. *Journal of Catalysis* **2019,** *370*, 372-377.
34. Maccarrone, M. J.; Lederhos, C. R.; Torres, G.; Betti, C.; Coloma-Pascual, F.; Quiroga, M. E.; Yori, J. C., Partial hydrogenation of 3-hexyne over low-loaded palladium mono and bimetallic catalysts. *Applied Catalysis A: General* **2012,** *441–442*, 90-98.
35. Lederhos, C. R.; Badano, J. M.; Quiroga, M. E.; L'Argentière, P. C.; Coloma-Pascual, F., Influence of ni addition to a low-loaded palladium catalyst on the selective hydrogenation of 1-heptyne. *Química Nova* **2010,** *33*, 816-820.
36. Mäki-Arvela, P.; Murzin, D. Y., Effect of catalyst synthesis parameters on the metal particle size. *Applied Catalysis A: General* **2013,** *451*, 251-281.
37. Liu, Y.; Zhao, J.; He, Y.; Feng, J.; Wu, T.; Li, D., Highly efficient PdAg catalyst using a reducible Mg-Ti mixed oxide for selective hydrogenation of acetylene: Role of acidic and basic sites. *Journal of Catalysis* **2017,** *348*, 135-145.
38. Lindlar, H.; Dubuis, R., Palladium Catalyst for Partial Reduction of Acetylenes. In *Organic Syntheses*, John Wiley & Sons, Inc.: 2003.
39. Lindlar, H., Ein neuer Katalysator für selektive Hydrierungen. *Helvetica Chimica Acta* **1952,** *35* (2), 446-450.
40. He, Y.; Fan, J.; Feng, J.; Luo, C.; Yang, P.; Li, D., Pd nanoparticles on hydrotalcite as an efficient catalyst for partial hydrogenation of acetylene: Effect of support acidic and basic properties. *Journal of Catalysis* **2015,** *331*, 118-127.
41. Maccarrone, M. J.; Torres, G. C.; Lederhos, C.; Betti, C.; Badano, J. M.; Quiroga, M. n.; Yori, J., Kinetic Study of the Partial Hydrogenation of 1-Heptyne over Ni and Pd Supported on Alumina. In *Hydrogenation*, Karamé, I., Ed. InTech: Rijeka, 2012; p Ch. 07.
42. Cao, Y.; Sui, Z.; Zhu, Y.; Zhou, X.; Chen, D., Selective Hydrogenation of Acetylene over Pd-In/Al2O3 Catalyst: Promotional Effect of Indium and Composition-Dependent Performance. *ACS Catalysis* **2017,** *7* (11), 7835-7846.
43. Anderson, J. A.; Mellor, J.; Wells, R. P. K., Pd catalysed hexyne hydrogenation modified by Bi and by Pb. *Journal of Catalysis* **2009,** *261* (2), 208-216.
44. Lederhos, C. R.; L'Argentière, P. C.; Fígoli, N. S., 1-Heptyne Selective Hydrogenation over Pd Supported Catalysts. *Industrial & Engineering Chemistry Research* **2005,** *44* (6), 1752-1756.
45. Silva, F. P. d.; Rossi, L. M., Palladium on magnetite: magnetically recoverable catalyst for selective hydrogenation of acetylenic to olefinic compounds. *Tetrahedron* **2014,** *70* (20), 3314-3318.
46. Boronoev, M. P.; Zolotukhina, A. V.; Ignatyeva, V. I.; Terenina, M. V.; Maximov, A. L.; Karakhanov, E. A., Palladium Catalysts Based on Mesoporous Organic Materials in Semihydrogenation of Alkynes. *Macromolecular Symposia* **2016,** *363* (1), 57-63.
47. Liprandi, D. A.; Cagnola, E. A.; Quiroga, M. E.; L'Argentière, P. C., Influence of the Reaction Temperature on the 3-Hexyne Semi-Hydrogenation Catalyzed by a Palladium(II) Complex. *Catalysis Letters* **2009,** *128* (3), 423-433.

48. Furukawa, S.; Komatsu, T., Selective Hydrogenation of Functionalized Alkynes to (E)-Alkenes, Using Ordered Alloys as Catalysts. *ACS Catalysis* **2016,** *6* (3), 2121-2125.
49. Liprandi, D.; Quiroga, M.; Cagnola, E.; L'Argentière, P., A New More Sulfur-Resistant Rhodium Complex as an Alternative to the Traditional Wilkinson's Catalyst. *Industrial & Engineering Chemistry Research* **2002,** *41* (19), 4906-4910.
50. Semagina, N.; Grasemann, M.; Xanthopoulos, N.; Renken, A.; Kiwi-Minsker, L., Structured catalyst of Pd/ZnO on sintered metal fibers for 2-methyl-3-butyn-2-ol selective hydrogenation. *Journal of Catalysis* **2007,** *251* (1), 213-222.
51. Sadeghpour, P.; Haghighi, M., High-temperature and short-time hydrothermal fabrication of nanostructured ZSM-5 catalyst with suitable pore geometry and strong intrinsic acidity used in methanol to light olefins conversion. *Advanced Powder Technology* **2018,** *29* (5), 1175-1188.
52. Asthana, S.; Samanta, C.; Bhaumik, A.; Banerjee, B.; Voolapalli, R. K.; Saha, B., Direct synthesis of dimethyl ether from syngas over Cu-based catalysts: Enhanced selectivity in the presence of MgO. *Journal of Catalysis* **2016,** *334*, 89-101.
53. Auroux, A.; Monaci, R.; Rombi, E.; Solinas, V.; Sorrentino, A.; Santacesaria, E., Acid sites investigation of simple and mixed oxides by TPD and microcalorimetric techniques. *Thermochimica Acta* **2001,** *379* (1), 227-231.
54. Topsøe, N.-Y.; Pedersen, K.; Derouane, E. G., Infrared and temperature-programmed desorption study of the acidic properties of ZSM-5-type zeolites. *Journal of Catalysis* **1981,** *70* (1), 41-52.
55. Zakaria, Z. Y.; Linnekoski, J.; Amin, N. A. S., Catalyst screening for conversion of glycerol to light olefins. *Chemical Engineering Journal* **2012,** *207-208*, 803-813.
56. Feng, J.-T.; Ma, X.-Y.; Evans, D. G.; Li, D.-Q., Enhancement of Metal Dispersion and Selective Acetylene Hydrogenation Catalytic Properties of a Supported Pd Catalyst. *Industrial & Engineering Chemistry Research* **2011,** *50* (4), 1947-1954.
57. Ma, X.-Y.; Chai, Y.-Y.; Evans, D. G.; Li, D.-Q.; Feng, J.-T., Preparation and Selective Acetylene Hydrogenation Catalytic Properties of Supported Pd Catalyst by the in Situ Precipitation−Reduction Method. *The Journal of Physical Chemistry C* **2011,** *115* (17), 8693-8701.
58. Brunelle, J. P., Preparation of catalysts by metallic complex adsorption on mineral oxides. In *Pure and Applied Chemistry*, 1978; Vol. 50, p 1211.
59. Paryjczak, T.; Szymura, J. A., Electron microscopic and chemisorption comparison studies on the metal dispersion of Pd, Rh, and Ir supported catalysts. *Zeitschrift für anorganische und allgemeine Chemie* **1979,** *449* (1), 105-114.
60. Ferrer, V.; Moronta, A.; Sánchez, J.; Solano, R.; Bernal, S.; Finol, D., Effect of the reduction temperature on the catalytic activity of Pd-supported catalysts. *Catalysis Today* **2005,** *107–108*, 487-492.
61. Badano, J. M.; Quiroga, M.; Betti, C.; Vera, C.; Canavese, S.; Coloma-Pascual, F., Resistance to Sulfur and Oxygenated Compounds of Supported Pd, Pt, Rh, Ru Catalysts. *Catalysis Letters* **2010,** *137* (1), 35-44.
62. Scheidema, M. N.; Taskinen, P., Decomposition Thermodynamics of Magnesium Sulfate. *Industrial & Engineering Chemistry Research* **2011,** *50* (16), 9550-9556.
63. L'Vov, B. V., Mechanism of thermal decomposition of alkaline-earth carbonates. *Thermochimica Acta* **1997,** *303* (2), 161-170.

64. Padeste, C.; Reller, A.; Oswald, H. R., The influence of transition metals on the thermal decomposition of calcium carbonate in hydrogen. *Materials Research Bulletin* **1990,** *25* (10), 1299-1305.
65. Wagner, C. D.; Muilenberg, G. E., *Handbook of X-ray Photoelectron Spectroscopy: A Reference Book of Standard Data for Use in X-ray Photoelectron Spectroscopy*. Perkin-Elmer: 1979.
66. NIST X-ray photoelectron spectroscopy database NIST standard reference database 20, Version 3.5 (Web version), National Institute of Standards and Technology, USA, 2007.
67. Tripathi, B.; Paniwnyk, L.; Cherkasov, N.; Ibhadon, A. O.; Lana-Villarreal, T.; Gómez, R., Ultrasound-assisted selective hydrogenation of C-5 acetylene alcohols with Lindlar catalysts. *Ultrasonics Sonochemistry* **2015,** *26*, 445-451.
68. D.F. Shriver; Atkins, P. W.; Langford, C. H., *Inorganic Chemistry*. 3rd ed ed.; New York, 1994.
69. Markov, P. V.; Turova, O. V.; Mashkovsky, I. S.; Khudorozhkov, A. K.; Bukhtiyarov, V. I.; Stakheev, A. Y., Size effect in the liquid phase semihydrogenation of substituted alkynes over supported Pd/Al2O3 catalysts. *Mendeleev Communications* **2015,** *25* (5), 367-369.
70. Zhang, H.; Yang, Y.; Dai, W.; Lu, S.; Yu, H.; Ji, Y., Size-controlled Pd Nanoparticles Supported on α-Al2O3 as Heterogeneous Catalyst for Selective Hydrogenation of Acetylene. *Chinese Journal of Chemical Engineering* **2014,** *22* (5), 516-521.
71. Vilé, G.; Almora-Barrios, N.; Mitchell, S.; López, N.; Pérez-Ramírez, J., From the Lindlar Catalyst to Supported Ligand-Modified Palladium Nanoparticles: Selectivity Patterns and Accessibility Constraints in the Continuous-Flow Three-Phase Hydrogenation of Acetylenic Compounds. *Chemistry – A European Journal* **2014,** *20* (20), 5926-5937.
72. Teschner, D.; Vass, E.; Hävecker, M.; Zafeiratos, S.; Schnörch, P.; Sauer, H.; Knop-Gericke, A.; Schlögl, R.; Chamam, M.; Wootsch, A.; Canning, A. S.; Gamman, J. J.; Jackson, S. D.; McGregor, J.; Gladden, L. F., Alkyne hydrogenation over Pd catalysts: A new paradigm. *Journal of Catalysis* **2006,** *242* (1), 26-37.
73. Crespo-Quesada, M.; Dykeman, R. R.; Laurenczy, G.; Dyson, P. J.; Kiwi-Minsker, L., Supported nitrogen-modified Pd nanoparticles for the selective hydrogenation of 1-hexyne. *Journal of Catalysis* **2011,** *279* (1), 66-74.

Caption to Figures

Figure 1. TPD-Py results. a) Supports. b) Catalysts.

Figure 2. TEM images and particle size distribution of the catalysts.

Figure 3. H_2-TPR traces of Pd/Al_2O_3, Pd/Al_2O_3–Mg and $Pd/CaCO_3$.

Figure 4. XPS spectra of the Pd *3d* region of all catalysts. Mg *2p* of Pd/Al_2O_3-Mg. Pb *4f* of the Lindlar[34] catalyst.

Figure 5. X-ray diffractograms of the catalysts.

Figure 6. (a) Total Conversion of 1-Heptyne (%) vs. Time (min) and (b) Selectivity to 1-Heptene (%) vs. Total Conversion (%) for Pd/Al_2O_3 (♦), Pd/Al_2O_3–Mg (▲), $Pd/CaCO_3$ (■) and Lindlar (○).

Figure 7. (a) Total Conversion of 1-Pentyne (%) vs. Time (min) and (b) Selectivity to 1-Pentene (%) vs. Total Conversion (%) for Pd/Al_2O_3 (♦), Pd/Al_2O_3–Mg (▲), $Pd/CaCO_3$ (■) and Lindlar (○).

Figure 8. (a) Total Conversion of 1-Pentyne (%) vs. Time (min), and (b) Selectivity to 1-Pentene (%) vs. Total Conversion (%) during the hydrogenation of the 1-Pentyne/1-Pentene mixture (30:70 $\%^{v}/_{v}$), for Pd/Al_2O_3 (♦), Pd/Al_2O_3–Mg (▲), $Pd/CaCO_3$ (■) and Lindlar (○).

Figure 9. Concentration of reactants and products (mol L^{-1}) as a function of time (min). Hydrogenation of a 1-Pentyne/1-Pentene mixture (30:70 $^{v}/_{v}$).

Scheme 1. Schematic drawing of simultaneous proton and ion-exchange on alumina Brönsted sites during $MgSO_4$ impregnation.

Scheme 2. Schematic drawing of simultaneous proton and ion-exchange on alumina free or modified during the impregnation of $[Pd(NH_3)_4]^{2+}$ in ammonia media.

Caption to Tables

Table 1. Results of N_2 physisorption isotherms of supports

Table 2. TPD-Py results.

Table 3. Metal loading as determined by ICP. Average particle size (d_{TEM}) and dispersion (D) from TEM microscopy. XPS results.

Table 4. Comparison of catalytic results.

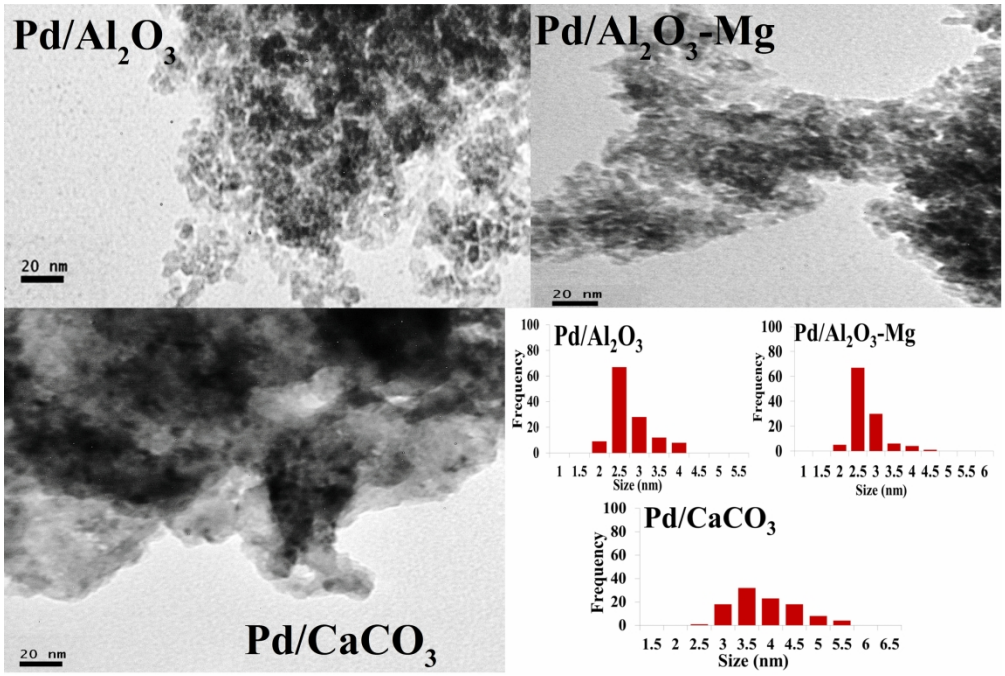

Figure 2.

254x170mm (300 x 300 DPI)

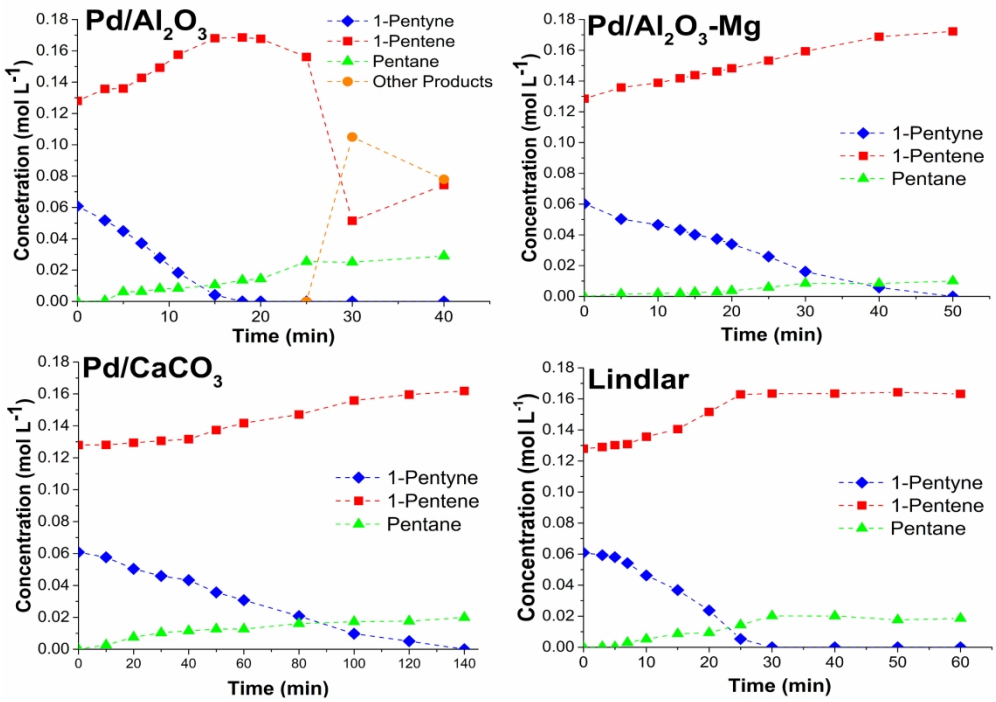

Figura 9.

254x177mm (300 x 300 DPI)

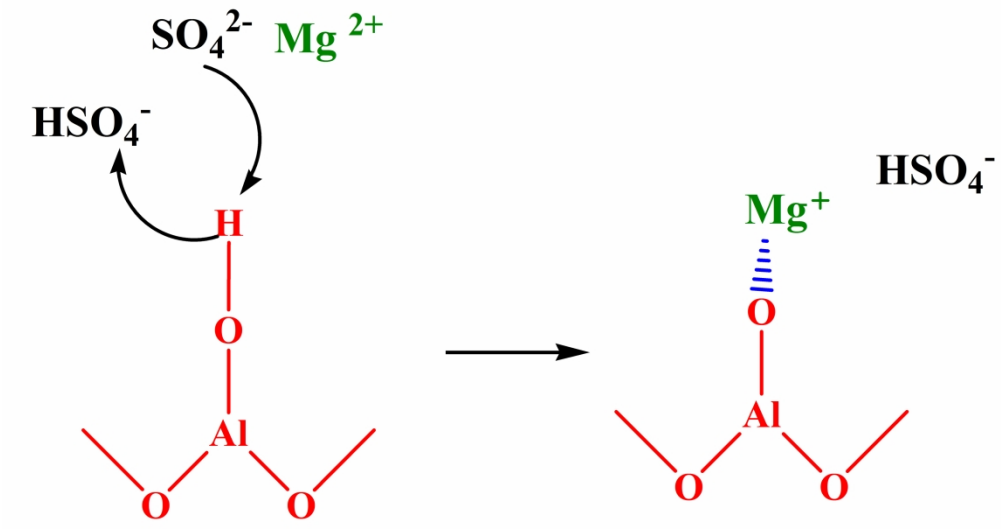

Scheme 1.

287x152mm (300 x 300 DPI)

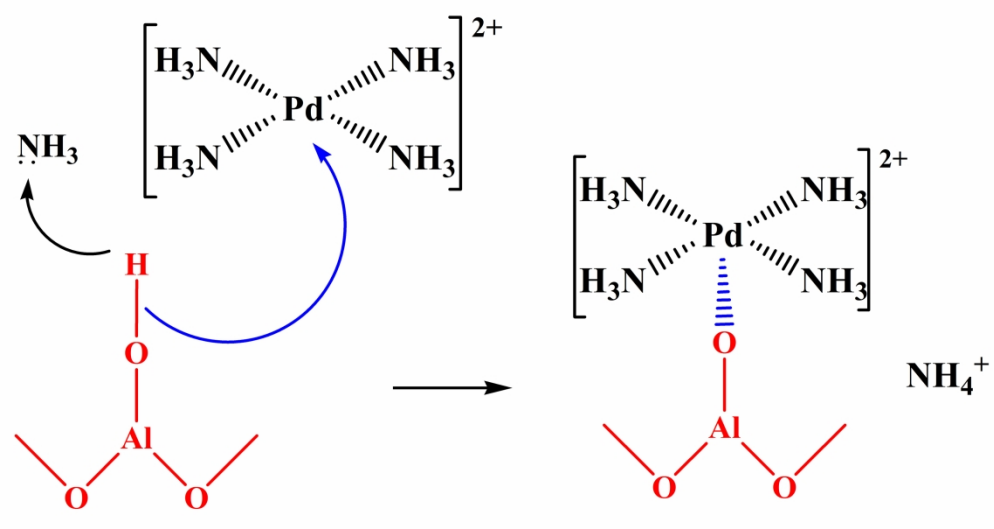

Scheme 2.

287x152mm (300 x 300 DPI)

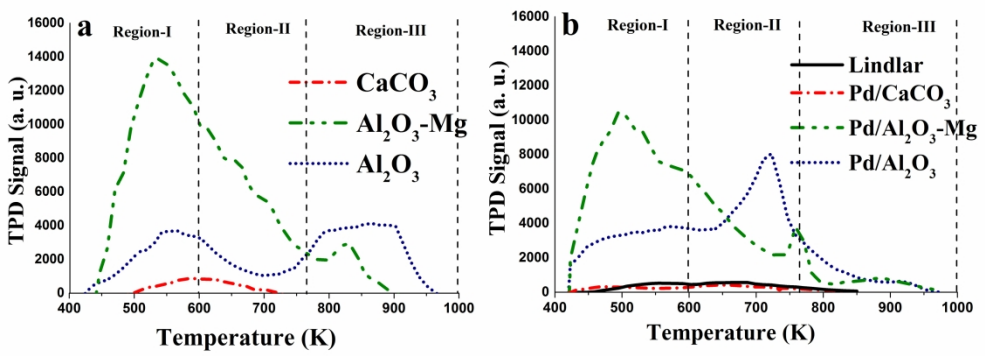

Figure 1.

304x109mm (300 x 300 DPI)

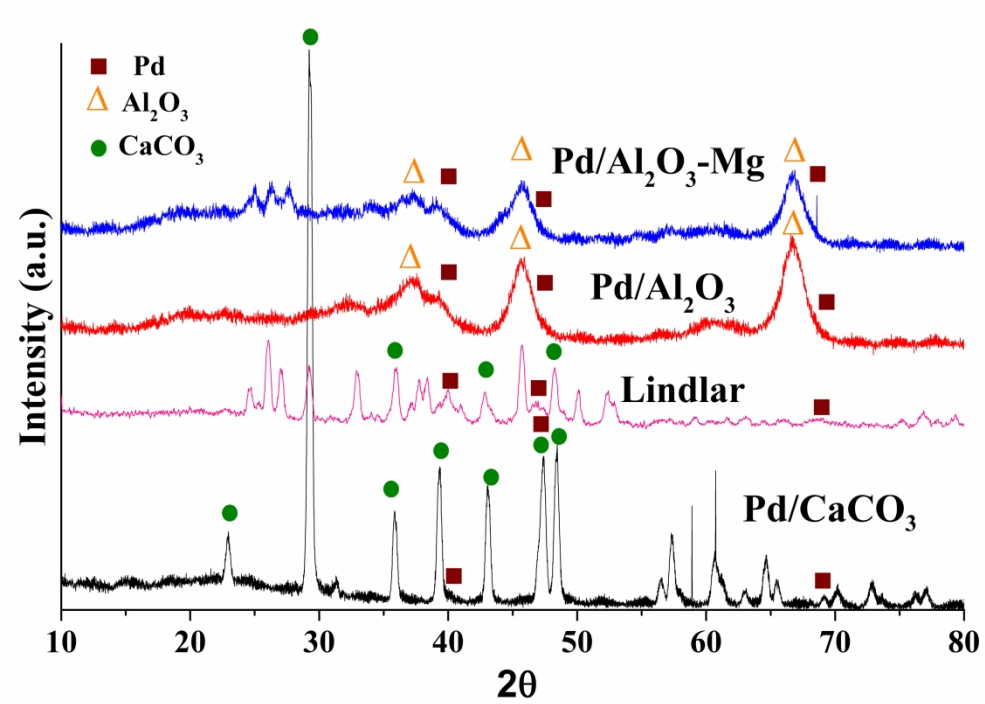

Figure 5.

286x201mm (300 x 300 DPI)

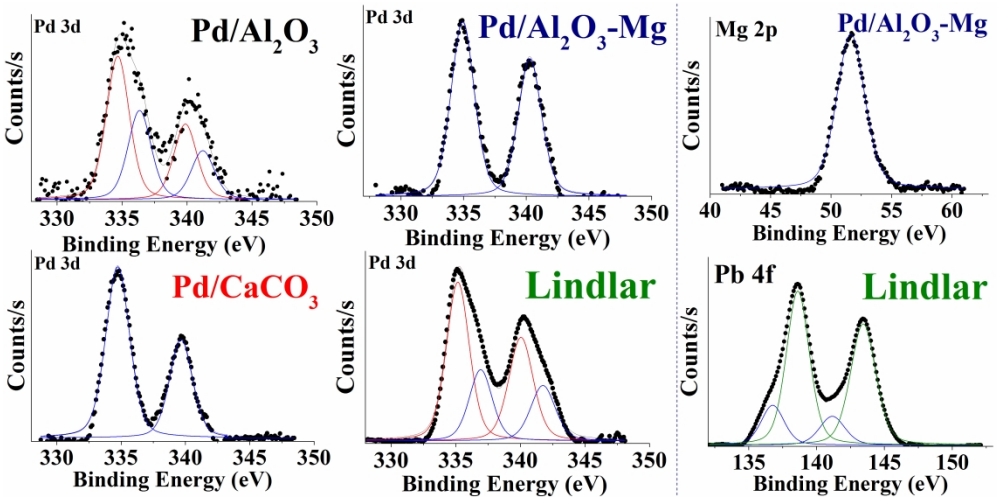

Figura 4.

406x201mm (300 x 300 DPI)

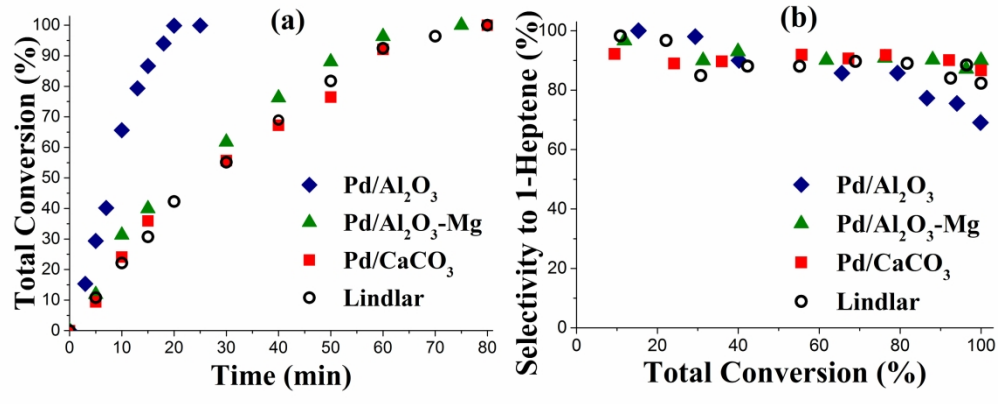

Figure 6

279x114mm (300 x 300 DPI)

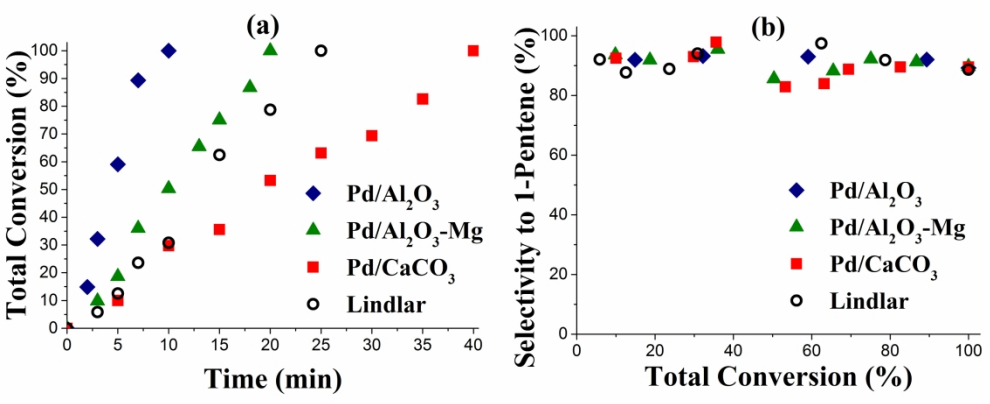

Figure 7

279x114mm (300 x 300 DPI)

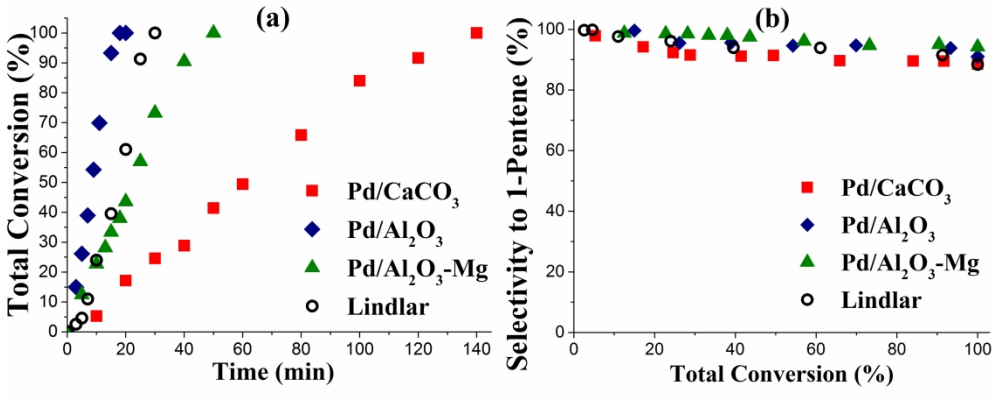

Figure 8

279x114mm (300 x 300 DPI)

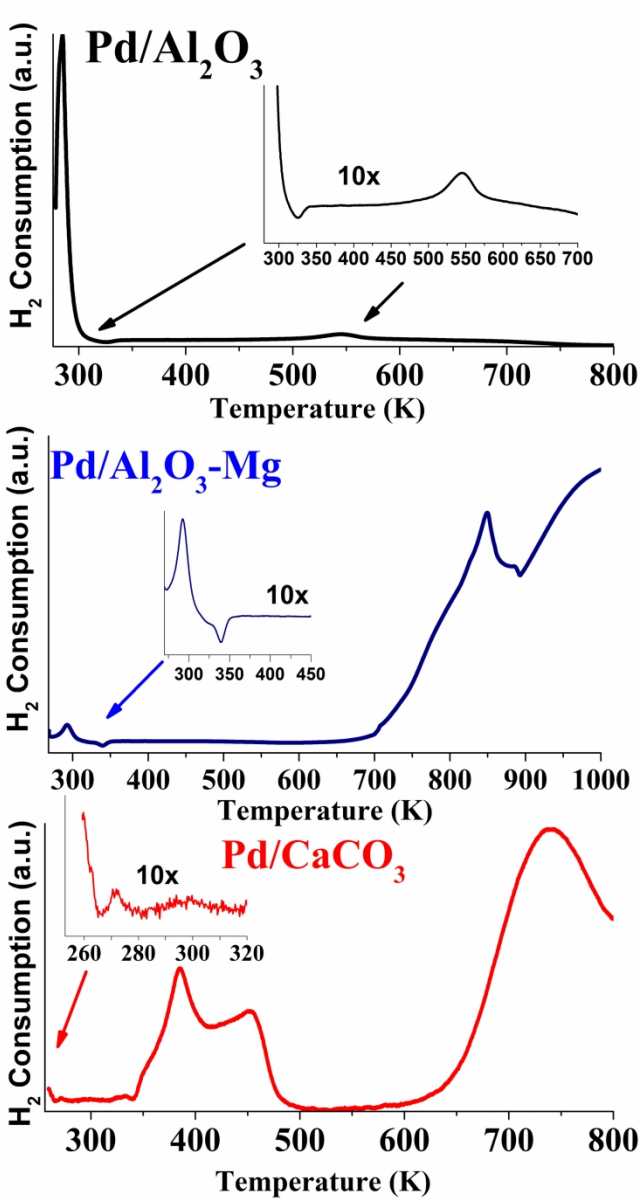

Figure 3.

149x279mm (300 x 300 DPI)